DESIGN AND ANALYSIS OF AN ELECTRIC ATTACHMENT FOR PROPELLING A WHEELCHAIR

_____

A Final Year Project Report

Presented to

SCHOOL OF MECHANICAL & MANUFACTURING ENGINEERING

Department of Mechanical Engineering

NUST

ISLAMABAD, PAKISTAN

_____

In Partial Fulfillment

of the Requirements for the Degree of

Bachelors of Mechanical Engineering

_____

by

Sunia Tanweer

Syed Muhammad Faraz Hussain Kazmi

June 2021

EXAMINATION COMMITTEE

We hereby recommend that the final year project report prepared under our supervision by:

SUNIA TANWEER   216639.

SYED MUHAMMAD FARAZ HUSSAIN KAZMI   207840

Titled: "DESIGN AND ANALYSIS OF AN ELECTRIC ATTACHMENT FOR PROPELLING A WHEELCHAIR" be accepted in partial fulfillment of the requirements for the award of BACHELORS OF MECHANICAL ENGINEERING degree with grade ___

Supervisor: Aamir Mubashar, Professor Department of Mechanical Engineering, SMME	Dated: /06/2021
Committee Member: Jawad Aslam, Assistant Professor Department of Mechanical Engineering, SMME	Dated: /06/2021
Committee Member: Emad Uddin, Assistant Professor Department of Mechanical Engineering, SMME	Dated: /06/2021

_____   _____

(Head of Department)   ./06/2021

COUNTERSIGNED

Dated: _____   _____

(Dean / Principal)

i

ABSTRACT

Over the span of the last couple of years, great strides have been made in the domain of assistive technology for the paraplegic community. Several of these advancements pertain to devices energized through various sources such as dry batteries and solar cells and propelled through electric motors. These devices, called power attachments, are used in conjunction with manual wheelchairs to enhance and supplement their mobility while minimizing the energy input from the user.

While immense attention has been given to the research and development of such power attachments, few to no attempts have been made at developing these for an inexpensive rate for maximizing the user base of such products. These attachments have a median cost of nearly PKR 0.5 million and are virtually inaccessible to the vast majority of Pakistani populace. This thesis aims to reduce this cost to at least one-tenth of its value and develop a cost-efficient power attachment within the buying power of Pakistani community.

The final product of this thesis is a high-speed power attachment capable of being connected to a standard Pakistani wheelchair. This product has a range greater than the major market contenders and a cost lower than them.

ACKNOWLEDGMENTS

ORIGINALITY REPORT

iv

7 "Squeeze the Lemon: Balancing as a Way to Use Every Drop of Energy in a Lithium-Ion Battery", Lecture Notes in Electrical Engineering, 2016.
Publication

<1 %

8 Nakamoto, H.. "In-plane impact behavior of honeycomb structures filled with linearly arranged inclusions", International Journal of Impact Engineering, 200908
Publication

<1 %

9 data.crossmedia.fi
Internet Source

<1 %

10 Chen, F.. "Stress distribution and dimensional changes in chromatographic columns", Journal of Chromatography A, 20050812
Publication

<1 %

11 Ikuo Tobinaga, Takeshi Ishihara. "A study of action point correction factor for L-type flanges of wind turbine towers", Wind Energy, 2018
Publication

<1 %

12 Submitted to University of Wollongong
Student Paper

<1 %

13 docs.trb.org
Internet Source

<1 %

14 www.cltsfoundation.org
Internet Source

<1 %

15 Nebbali, R.. "Dynamic simulation of the distributed radiative and convective climate within a cropped greenhouse", Renewable Energy, 201207
Publication

<1%

16 openaccess.city.ac.uk
Internet Source

<1%

17 qdoc.tips
Internet Source

<1%

18 www.chem.uu.nl
Internet Source

<1%

19 Kemper, H.. "An alternative presentation of the effects of the stress-ratio on the fatigue threshold", Engineering Fracture Mechanics, 1989
Publication

<1%

20 Prashant Prakash, Sanjay Kumar Jha, Shree Prakash Lal. "Numerical investigation of stirred zone shape and its effect on mechanical properties in friction stir welding process", Welding in the World, 2019
Publication

<1%

21 www.omcdesign.com
Internet Source

<1%

Exclude quotes	Off	Exclude matches	Off
Exclude bibliography	On		

TABLE OF CONTENTS

LIST OF TABLES

LIST OF FIGURES

ABBREVIATIONS

FEA	Finite Element Analysis
km/h	Kilometers per hour
m/s	Meters per second
m/s^2	Meters per second per second
V	Volts
Ah	ampere-hour
Wh	watt-hour
W	Watts
kg	Kilograms
mph	miles per hour
km	Kilometers
PKR	Pakistani Rupees
USD	United States Dollars
MPa	Megapascals
GPa	Gigapascals
Pa	pascals
N/A	Not Applicable
CAD	Computer Aided Design
LiFePO4	Lithium Iron Phosphate
kg/m^3	Kilogram per cubic meter
^oC	degrees Celsius
3D	Three Dimensional

DPDT	Double Pole Double Throw
CAE	Computer Aided Engineering
SI	System International
CoG	Center of Gravity
N	newtons
kPa	Kilo-pascals
mm	Millimeters
FoS	Factor of Safety
HS	Harmonized System (international coding system to classify trade products)
MIG	Metal Inert Gas Welding
ERW	Electrical Resistance Welding
TIG	Tungsten Inert Gas Welding
RPM	Revolutions per Minute
abs	Absolute value
rad	Radians

NOMENCLATURE

S_c	Critical Stress (MPa)
σ_y	Yield Stress (MPa)
σ_1	Maximum Principal Stress (MPa)
σ_2	Minimum Principal Stress (MPa)
FoS	Factor of Safety
σ_{mises}	Von Mises Stress (MPa)
v	Velocity (m/s)
ρ_{air}	Density of air (kg/m^3)
A_f	Frontal Area (m^2)
μ	Coefficient of Rolling Friction
m	Total Mass (kg)
C_d	Drag Coefficient
R	Range (m) or Radius at Interference Surface (m)
ρ_{air}	Density of air (kg/m^3)
V	Voltage of Battery/Motor (V)
$\emptyset$	Efficiency of Motor (%)
ω	Rotational Speed of Motor (RPM or rad/s)
F_d	Drag Force (N)
f	Frictional Force (N)
F	Total Tractive Force (N)
P_{elec}	Electrical Power (W)

P_{bat}	Battery Power (W)
E	Energy Stored in Battery (Wh)
C_{bat}	Battery Capacity (Ah)
D	Diameter (m)
k	Coefficient of Thermal Conductivity (Wm^{-1}K^{-1})
h	Convection Coefficient (Wm^{-2}K^{-1})
T_s	Surface Temperature (K or ^{o}C)
T_b	Battery Temperature (K or ^{o}C)
T_∞	Ambient Temperature (K or ^{o}C)
q	Heat Flux (Wm^{-2})
ε	Emissivity
σ	Boltzmann's Constant (5.67*10^{-8} Wm^{-2}K^{-4}) or Stress due to Interference (MPa)
t	Thickness (m)
r	Radius (m)
A	Cross-sectional Area (m^2)
π	Pi
P	Force from Wheelchair on Bolt
$\sigma_{b,avg}$	Average Bearing Stress in Bolt (MPa)
δ	Interference (mm)
r_i	Internal Radius of the Internal Part of Interference Fit (m)
r_o	External Radius of the External Part of Interference Fit (m)
E_i	Elastic Modulus of the Internal Part of Interference Fit (GPa)
E_o	Elastic Modulus of the External Part of Interference Fit (GPa)

v_i	Poisson's Ratio of the Internal Part of Interference Fit
v_o	Poisson's Ratio of the External Part of Interference Fit
$\sigma_{y,i}$	Yield Stress of the Internal Part of Interference Fit (MPa)
$\sigma_{y,o}$	Yield Stress of the External Part of Interference Fit (MPa)
FoS_i	Factor of Safety of the Internal Part of Interference Fit
FoS_o	Factor of Safety of the External Part of Interference Fit
$F_R(\tau\alpha)$	Conversion factor (optical efficiency of solar collector)

CHAPTER 1: INTRODUCTION

Wheelchairs are the most frequently used assistive devices used by paraplegics to aid mobility. They come in a wide variety of formats to meet the needs of the user such as; being lightweight, portable, low cost, etc. Based on propulsion source, wheelchairs can be classified into three broad categories, as shown in Fig 1.
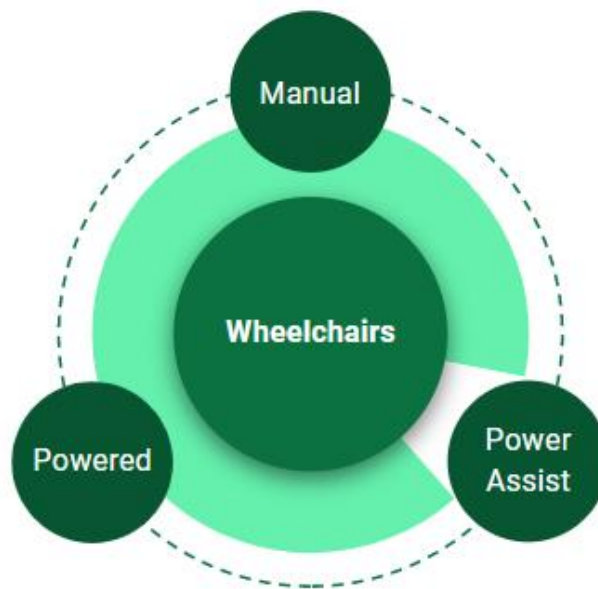
Figure 1: Categories of wheelchairs based on the type of propulsion.

While manual wheelchairs restrict mobility of the user due to low propulsive force which comes from the user's muscular energy, powered wheelchairs restrict the mobility due to their high weight and inability to traverse difficult and/or irregular terrains such as stairs. A power-assisted wheelchair combines the best characteristics of manual and powered wheelchairs. Although fulfilling the need of flexibility, ease of use and speed control, the available power attachments fall short in the cost domain so much that it is virtually impossible for a low-income family to purchase them. A preliminary cost analysis puts the three categories in the cost ranges as shown in Fig 2.

Price Range for Wheelchairs
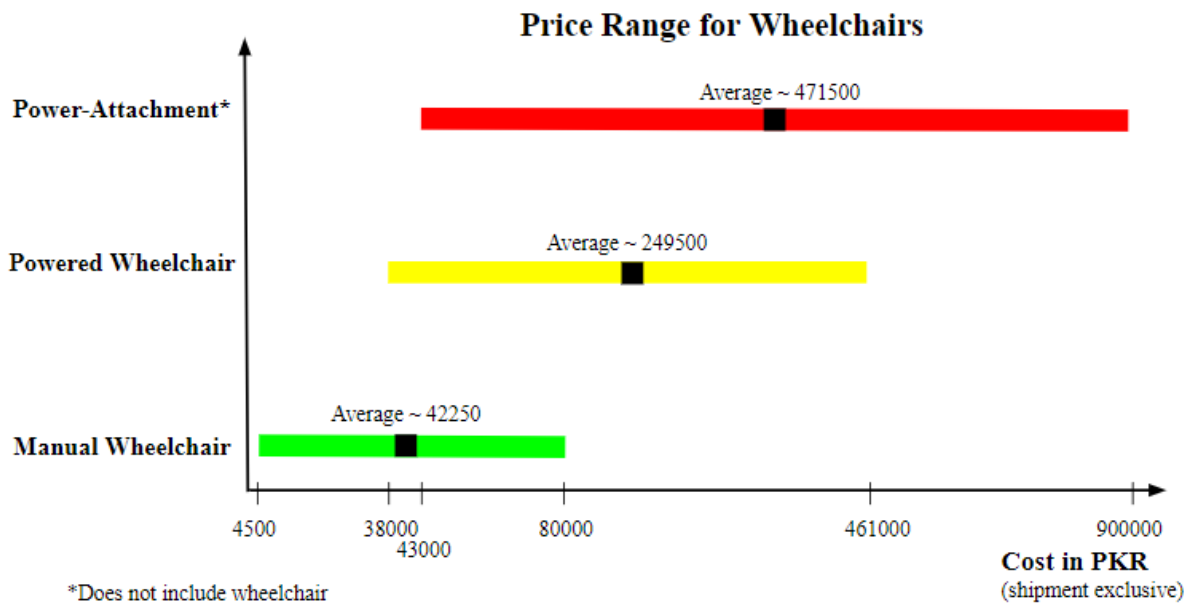
Figure 2: Price ranges for three categories of wheelchairs estimated using [1-5]

Hence, to avail the flexibility provided by a power-assist wheelchair, this senior year project sought to settle the problem of designing a cost-effective power attachment which can fit a standard wheelchair available in local market while being uncompromising in user comfort.

Project Objectives

Manual wheelchairs do not travel fast for obvious reasons while most powered wheelchairs have a maximum speed of nearly 11 km/h, such as [6]. On the other hand, power-assist attachments have a thrilling maximum speed of 40 km/h, such as [7], which comes with the caveat of its high cost. Thus, it was decided that it is best to focus on a hybrid and design a power-assist attachment with a speed higher than powered wheelchairs and a cost lower than most power-assist attachments already available in the market. The objectives decided for the project are given in Table 1.

2

Table 1: Design specifications for the powered wheel chair attachment.

Feature	Specification
Cost	Minimize the cost to less than PKR 50,000.
Speed	Provide a minimum speed of 15 km/h which can be controlled.
Range	Provide a minimum range of 20 km to minimize charging frequency.
Comfort	Develop the design based on basic ergonomics for a human body.
Steering	Provide an easy steering control in contrast to manual wheelchairs.
Installation	Design the installation method to minimize required time and effort.
Weight/Portability	Minimize the attachment weight to less than 25 kg.

Project Management and Deliverables

The project was divided into multiple phases, as shown in Fig 3.
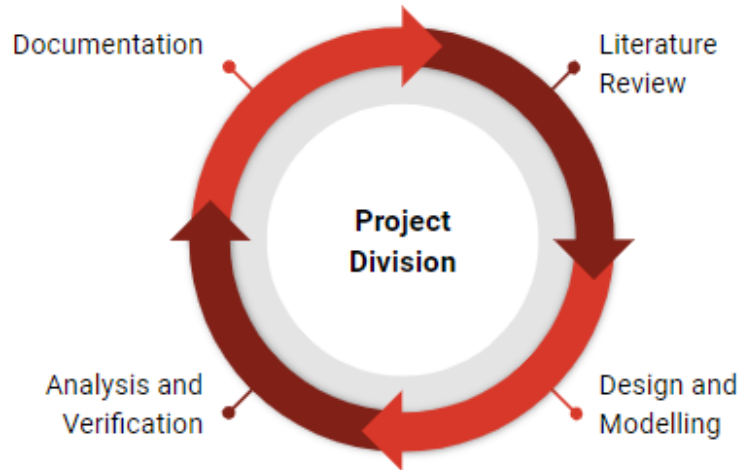
Figure 3: Project phases for design and development.

The first stage of the project, the literature review, included an in-depth comparison of different materials, batteries, motors and drive-configurations, etc. In the second phase, a number of concept designs were sketched and the best suited geometry was chosen as the

final design for modelling and analysis. In the third phase, the modelled design was analyzed structurally and dynamically against maximum loading conditions to verify its reliability and safety. The final phase revolved around the documentation of the project.

The project had four main deliverables, as shown in Fig 4.
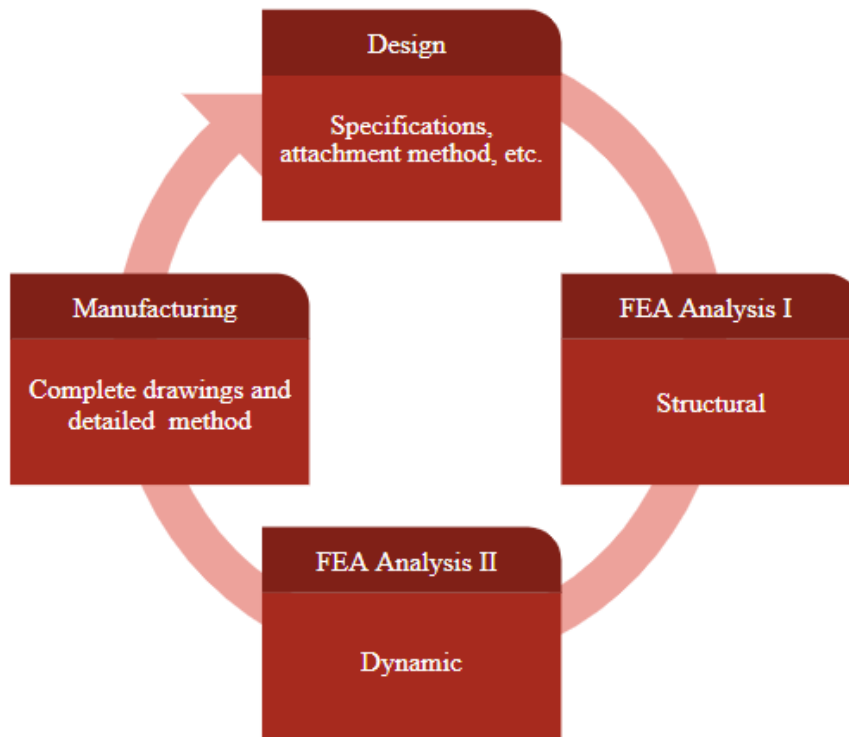
Figure 4: Project Deliverables

CHAPTER 2: LITERATURE REVIEW

A number of electrical attachments [2-8] for wheelchairs have been designed and manufactured to this day. This highlights the importance and complexity of this domain. This chapter involves a brief introduction to some of the popular designs available in the market, the need which our design fulfills and a comparison of the different options available to us for the multiple necessary components of our attachment, such as structural material, battery and motor type.

Available Designs

The following section discusses some of the popular commercially available power attachments for manual wheelchairs.

Firefly by Rio Mobility [9]:

Rio Mobility offers lightweight easy to attach design solutions to propel a wheelchair. A Lithium Ion 36V, 7Ah, 252 Wh battery is employed that gives around 15 miles per charge cycle. The frame is made up of Aluminum 6061 with a 12.5" X 3.0" tyre. The attachment is a front wheel drive with a 350W, 36V Geared brushless hub motor with reinforced steel gears. A top speed of 12 mph is attainable with the Firefly. A handlebar steering system is employed by the Firefly. The RIO Firefly (shown in Fig 5) has a base cost of PKR 400,000 [10] and nearly PKR 570,000 after shipping and import duty.

Figure 5: Firefly by Rio Mobility [10]

SmartDrive by Permobil [11]:

The SmartDrive, shown in Fig 6, is a compact design that powers the wheelchair from the back. It is equipped with a LiFePO4 – 36 V and 3.4 Ah battery that provides a range of 12 miles. The wheelchair is propelled by a 250W Brushless DC motor. The attachment does not come with a steering mechanism. The user steers using their hands and stalling the wheels of the wheelchair. The SmartDrive has a base price of around PKR 1,000,000 [12] which rises to PKR 1,390,000 after shipping and import taxes.

Figure 6: SmartDrive by Permobil [11]

Mini-2 by Batec Mobility [13]:

The Batec provides a compact, practical, versatile mobility solution and is one of the most popular products in the market. The chassis is made of 7005 Aluminium with a 36 V 500 W Brushless DC Motor for propulsion. It is equipped with a 9-11 Ah lithium battery, which gives a range of 30 - 40 km. It comes with 20" aluminium double-wall rims. The attachment is a front wheel drive and uses 20" tyres. The Batec Mini is shown in Fig 7 and generally weighs around 14.9 kg with a top speed of 25 km/h. It costs around PKR 1,100,000 [14] and around PKR 1,523,000 after shipping and taxes.

Figure 7: Mini-2 by Batec Mobility [13]

Pride Jazzy 600 ES by Pride Mobility [15]:

Pride Jazzy is an electric wheelchair which is not classified as an attachment. It is a standalone product that comes with a mid-wheel drive and achieves a top speed of 4 mph. It offers a range of 17 miles per charge and costs around PKR 600,000 [16] and PKR 843,000 after shipping and taxes. Fig 8 shows the Pride Jazzy 600 ES.

Figure 8: Pride Jazzy 600 ES by Pride Mobility [16]

Wheelchair Electric Handcy Kit by B.E. Appliances [8]:

Boneng Electric presents a simple and cost effective product that comes with a geared brushless motor of 250 W and options between a 36 or 48 V battery. The frame is made of stainless steel and the product weighs a total of 30 kg. The max speed attainable is around 20 km/hr. The Handcycle Kit, as shown in Fig 9, has a base cost of nearly PKR 44,000 and PKR 91,000 after shipping and taxes.

Figure 9: Wheelchair Electric Handcy Kit by Boneng Electric Appliances [8]

Electric Attachment by Blommestein et al. [17]:

A group of researchers from Santa Clara University designed a product, shown in Fig. 10 they deemed viable as a rear wheel drive. The Drive Unit was a gear reduction motor which came with added weight, a chain and an 8inch wheel. The attachment is clipped on using a clamp with a pin lock which is attached to the cross struts of the wheelchair. The throttle was designed to include a potentiometer and an Arduino board. 36V, 10 A-h lithium iron phosphate batteries were used which came in with a built in mount housing. A maximum speed of 4.5 mph was attainable on asphalt and a range of 8.9 miles per charge cycle.

Figure 10: Electric Attachment by Bloomestein et al. [17]

Comparison of Basic Components Required

The basic components and decisions required to develop an electric attachment are given in Fig 11 and discussed in the following sections.
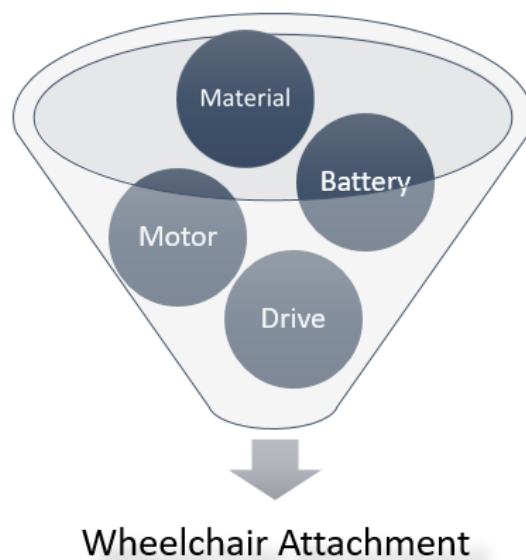
Figure 11: Basic components/decisions required to design an electric attachment

Material Selection:

A number of materials for the attachment's structure were investigated. Based on a preliminary analysis, four materials were shortlisted for in-depth scrutiny. These four materials were compared on the basis of four factors with emphasis on keeping both the cost and the density low. The comparison can be found in Table 2.

Table 2: Comparison of Different Materials Available for the Chassis

	Steel AISI 4340-O	Aluminum 6061-T6	Titanium Alloy (Ti6Al4V)	Carbon Fiber
Yield Strength (MPa)	472 [18]	276 [18]	830 [18]	3800 [18] (brittle)
Modulus of Elasticity (GPa)	207 [18]	69 [18]	114 [18]	230 [18]
Cost (PKR per kg)	110 [19]	400 [20]	~ 4560* [21]	10,100** [22]
Weldability	Friction [23]	Friction Stir [24], MIG [25], TIG [26]	MIG [27], Laser [28], Friction [29]	N/A
Density (kg/m^3)	7850 [18]	2700 [18]	4430 [18]	1780 [18]

* Cost calculated from USD 30 according to Eq (1-a).

** Cost calculated from INR 4800 according to Eq (1-b)

$$1\ USD = 152\ PKR \qquad (1\text{-}a)$$

$$1\ INR = 2.1\ PKR \qquad (1\text{-}b)$$

On the basis of yield strength as well as stiffness, carbon fiber appears to be the most favorable option. However, given that the load on the attachment will only be of an average male, the high yield strength of carbon fiber will not be required. A cost-to-benefit analysis suggests Aluminum 6061-T6 as the best option given its high strength to weight ratio and acceptable cost per kilogram. The material selection is shown in Fig 12.
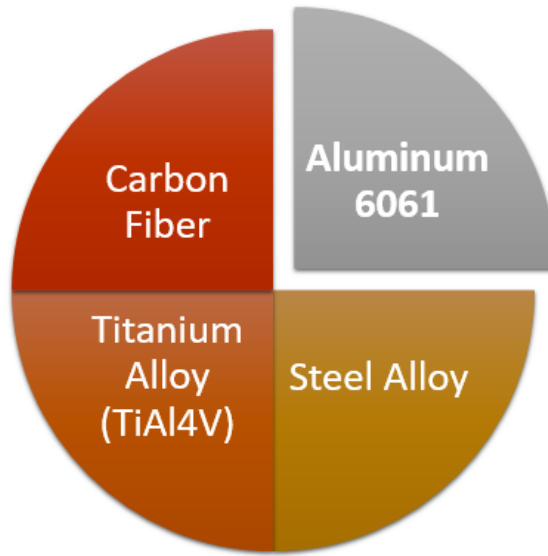
Figure 12: Preferred Material Selection

Battery Selection:

For similar power rating, a number of popular electric vehicle batteries were compared on the basis of four factors: endurance, weight, cost and explosion temperature with emphasis on keeping both the cost and the weight minimal. The comparison can be found in Table 3.

Table 3: Comparison of Different Batteries Available

	Lithium ion	**Lithium Polymer**	**Lithium Iron Phosphate**	**Sealed Lead Acid**
Endurance	< 1000 [30]	300-500 [31]	3000 [32]	200-300 [33]

Cost (USD)	45 [34]	600 [35]	320 [36]	75* [37]
Weight (kg)	2 [34]	2.15 [35]	6.8 [36]	5.8* [37]
Explosion Temperature (°C)	~ 66.5 [38]	~ 60 [39]	Safe [40]	Safe [41]

*Used for 3 batteries to normalize data against 36 V.

Based on the low cost and weight, Lithium-ion batteries are appropriate for our application. However, the associated safety hazard was a point of concern. A short heat transfer analysis was conducted to calculate the suitability of the battery. The calculations can be found in Appendix I. The final battery selection is shown in Fig 13.
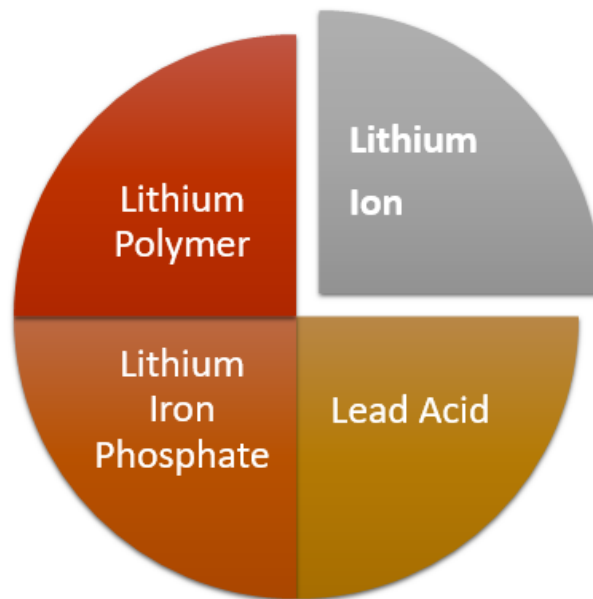
Figure 13: Preferred Battery Selection

Motor Selection:

The selection of motor was done on the sole factor of compactness. Hub motors enable the attachment to be compact in size, and appear to be the best choice for this case. The motor capacity, size and associated tire were later calculated based on our specified load requirements.

Drive Type Selection:

For any wheel-based vehicle, three drive types are possible: Front-wheel, mid-wheel and rear-wheel. Mid-wheel drive type was eliminated on the complexity of the design. Further elimination was done based on factors such as stability and ease of attachment, and can be found in Table 4.

Table 4: Comparison of different drive types.

	Front-Wheel Drive	*Rear-Wheel Drive*
Stability	Less stable (raises center of gravity)	More stable (lowers center of gravity)
Steering Configuration / Maneuverability	Handle-controlled	Hand-controlled
Easy of Attachment	Easy	Difficult

Prioritizing the comfort of the user, it was decided to design a front-wheel driven type wheelchair for its ease of attachment and better maneuverability.

CHAPTER 3: METHODOLOGY

In this chapter, the design process is discussed which led to an iterative modelling and analysis process for the attachment. The chapter begins with an introduction to the deciding factors in the design phase such as easy attachment method and basic ergonomics for user comfort. Then, the chapter briefly discusses the modelling phase. Later on, various loading conditions for analysis of the model, the results of the analyses and the final selections based on them are discussed. Finally, a simple scheme for manufacturing and assembling a working prototype is presented.

Design Considerations

The basic design of the attachment was produced keeping in mind several factors such as an easy mode of attachment with the wheelchair and maximum comfort of the user. Other considerations included the motivation to reduce the cost and product specifications such as maximum acceleration and speed.

Standard Wheelchair available in Local Market

The dimensions of the design were constrained based on the dimensions of a standard wheelchair available in the local market. An average male-sized wheelchair made of Aluminum alloy with rubber tires was chosen as the baseline and modelled using Dassault Systèmes' 3D CAD software *SolidWorks*, as shown in Fig. 14. The drawings of the wheelchair can be found in *Appendix II*. The dimensions of this wheelchair set the constraint for the width of the attachment and the length of its arms. The other specifications, such as the material of the tires being rubber, constrained the maximum speed which could be achieved without irreversibly damaging the rubber wheels.

Figure 14: CAD Model of a Standard Pakistani Wheelchair Made in SolidWorks

Ergonomics

Some basic ergonomics for maximum comfort for an average male-sized human body guided the design's dimensions. The two parameters considered were *handlebar rise* and *handlebar incline*, as shown in Fig. 15. Delfin et al. [42] concluded that the angle of the incline should be between 45 degrees and 54 degrees for maximal comfort of the user. This design uses 45 degrees angle of incline to provide space for a kickstand which would support the attachment when disconnected from the wheelchair. On the other hand, the handlebar rise was decided based on the average length of the male torso [43] and a straight body posture with horizontally stretched out arms following a classic (Dutch) biking position.
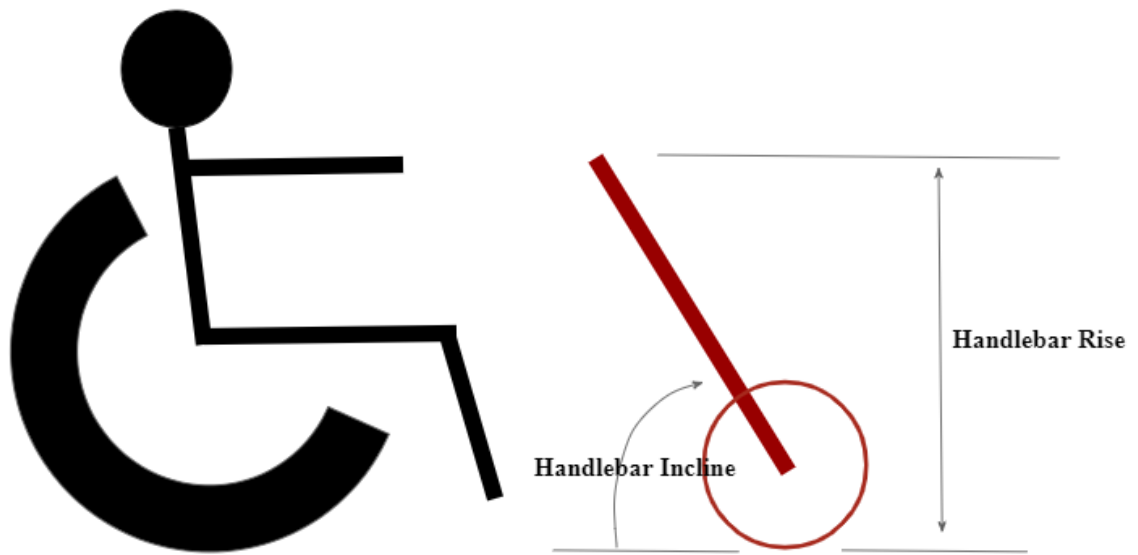
Figure 15: Handlebar Rise and Incline in an Attachment for Considering Ergonomics

Final Design Specifications

The final design specifications such as the battery capacity were based on the specifications acceptable for an average user without over or underdoing it. The specifications decided are given in Table 5.

Table 5: Specification Decided for the Attachment

Specification	Standard
Maximum Speed	20 km/h (5.55 m/s)
Maximum Acceleration	~ 6 m/s^2
Range	35 km

Failure Criterion

A number of failure theories have been proposed since times immemorial such as the Maximum Shear Stress (Tresca) Failure Criterion, Distortion Energy (Von Mises) Failure Criterion, Coulomb-Mohr's Theory of Failure and Maximum Normal Stress Theory [reference]. The former three are utilized for judging failure in ductile materials while the latter is associated with brittle materials. The major portion of the attachment, the steering and chassis, are composed of a metal alloy Aluminum 6061 which is fairly ductile in nature. Hence, any of the former three can be applied to judge failure of the attachment. While all theories are reasonably acceptable, Tresca theory tends to underestimate the failure stress leading to overestimation of the material requirement, as shown in Fig. 16. Therefore, it was decided to use von Mises Failure Criterion for this design.
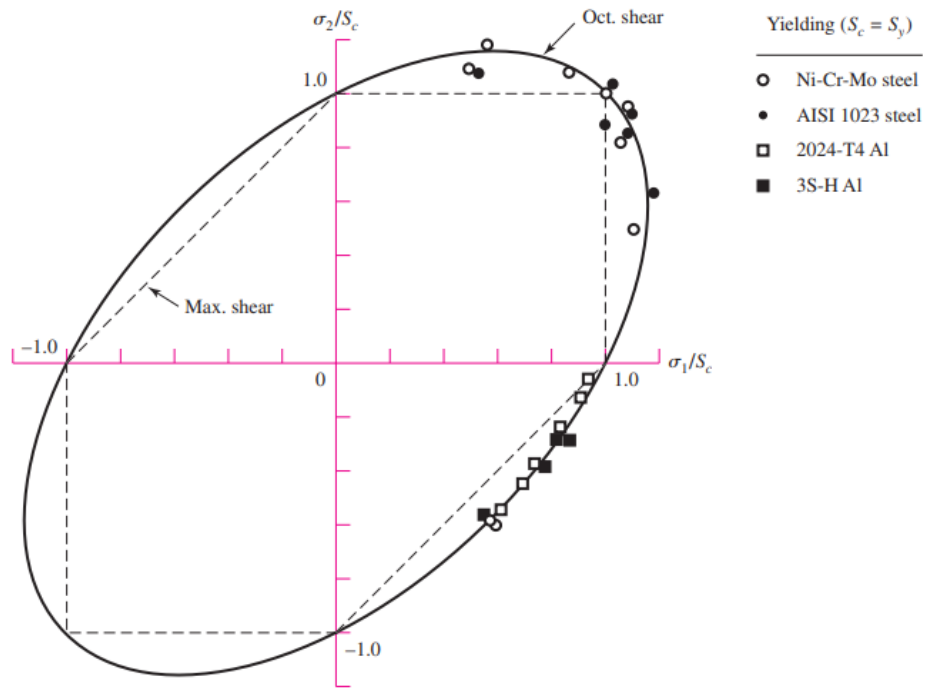
Figure 16: Failure Theories superimposed with Experimental Data [44]

Design Components

The main components of the design include steering with kickstand, bearing, chassis, battery in a battery holder, hub motor tire assembly, disc brakes, throttle, nuts and bolts. The final assembly is shown in Fig 17, followed by an exploded view in Fig 18.

Figure 17: Design of Power Attachment Modelled in SolidWorks

Figure 18: Exploded View of the Power Attachment

Steering Control

The steering portion, as shown in Fig. 19, consists of the handlebar, the throttle, the brake and holes for bolting the hub motor tire. A roller bearing push-fitted to this steering provides a rotational degree of freedom to it relative to the remaining chassis fixed to the wheelchair.

Figure 19: Steering of the Attachment

Method of Attachment to Wheelchair

The chassis, as shown in Fig 20, housing the roller bearing for the steering is fixed to the wheelchair through a pipe-clamp structure. This pipe clamp structure consists of a bolt and nut going through a U-shaped clamp. The arrangement can be seen in Fig 21.

Figure 20: Chassis Part which Connects to the Wheelchair

Throttle

All electric vehicles require a throttle to control the speed of the motor, and hence the speed of the vehicle. A throttle is in essence a variable-type resistor which changes the amount of current being passed to the motor by dint of which it alters the rotational speed of the motor. This arrangement can be efficiently replaced with a potentiometer to offset the cost of an off-the-shelf throttle by nearly 84% while using a double-push double-throw (DPDT) switch to reverse the direction of the motor. The circuit diagram connecting the potentiometer, the DPDT switch, the motor and the battery can be found in *Appendix III* for assistance. However, for ease of attachment, our design and cost analysis use a ready-made throttle instead.

Hub Motor

For compactness of design, a hub motor was preferred. Placed inside its rim, a hub motor has its shaft sticking outside which can be aligned inside the steering portion of the attachment and fixed in place using a nut. To conform to the battery voltage, a hub motor of 36V was selected with an appropriate rim size to match the size of the tire.

Tire

The pneumatic tire, made of rubber, was selected on the basis of two parameters: maximum speed requirement of the attachment and the hub motor's rotational speed. See *Appendix I* for calculations.

Disc Brakes

Manual wheelchairs use a combination of body force and wheel-locks to bring the wheelchair to a halt. While this system is suitable for a manual wheelchair having a low momentum, it is insufficient for wheelchairs powered through motors. Hub motor tires can be easily equipped with either one of disc brakes or rim brakes, however, disc brakes have been preferred for easier and safer braking [45]. Therefore, our model uses ready-made disc brakes easily available for hub motor tires.

Working of the Product

The product is intended for use once connected to the wheelchair by means of a bolt and nut, shown in Figure 21. Once seated properly, the user can start the motor through the throttle, which is also a controller of the attachment's speed. The handlebars can be used to control and vary the direction of the vehicle by utilizing the rotational freedom the roller bearing provides with respect to the wheelchair. A clutch installed on the handlebar provides access to the disc brakes and can be utilized for braking support, however, the speed can also be slowed down through the throttle albeit it being a more time taking process. Finally, once halted, the attachment can be removed from the wheelchair and supported through its kickstand. Once discharged, the battery can be removed from its housing, put to charge using the provided charger and placed back inside the housing.

Figure 21: Chassis Connected to the Wheelchair by dint of a Bolt and Nut

Finite Element Analysis (FEA)

Finite Element Analysis (FEA) is a numerical technique used to predict stresses and displacements in a structure by discretizing the domain into a mesh of small elements, whose individual behavior is calculated under the given loading conditions. Modelling of

the attachment's chassis was carried out using this method using Dassault Systèmes' commercially available FEA software Abaqus. The model, made in SolidWorks, was meshed, processed and post-processed using Abaqus CAE. SI units (kg, m and s) were consistently used throughout the process.

Load Division

Fig 22 shows the Center of Gravity (CoG) of the wheelchair-attachment assembly. The location of the CoG suggests no load from the user or the wheelchair on the attachment. Hence, user and wheelchair weight have not been considered in the FEA model. The only loads acting on the chassis are of the battery, the gravitational pull and the accelerative forces.

Center of Gravity (CoG)

Figure 22: Location of Center of Gravity of the System (80 kg added for user)

Model and Material Parameters

The FE model was a simplified version of the CAD model, where the bearing was replaced with a solid part and the entire structure was assumed to be one solid to avoid getting into tardy contact analyses. The model was reduced to a simple chassis, and hence was only used to estimate the stresses in the arms, steering and handlebar. The bearing stresses were calculated by hand later (see *Error Sources and Remedial Measures*). Keeping in mind the model assumptions, the FE simulations, in general, were only designed to rectify any yielding possible in the arm, neck and leg regions of the chassis. The accuracy of these simulations should be assumed minimal in the hotspot region, such as that of the interference fit between the bearing and the chassis, and hence, the FE results in those regions should be ignored.

The material tested was Aluminum 6061-T6, the properties of which used in the simulations can be found in Table 6 below.

Table 6: Material Properties used for Aluminum 6061-T6 in the Analysis

Properties	Values
Young's Modulus (GPa)	69.9
Poisson's Ratio	0.33
Density (kg/m³)	2700
Yield Stress (MPa)	276

Loading Conditions

The attachment was analyzed for a number of loading conditions, shown in Fig 23 below.
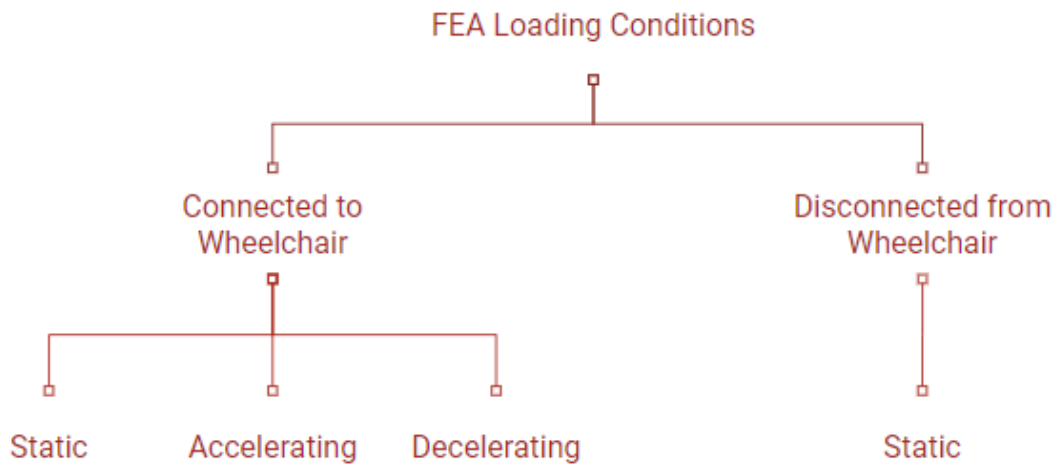
Figure 23: Load Cases Considered in the Analysis

In both static cases, the primary load was merely the weight of the battery modelled as a concentrated force directly below the battery's Center of Gravity. Zero displacement boundary conditions were applied wherever suitable, with a pretension force used for nuts and bolts. In both positive and negative acceleration cases, the battery weight was appended with accelerative forces on both the structure and the battery. An illustration of the loading conditions can be seen in Fig 24 below. In static case, the acceleration has been reduced to 0 m/s².
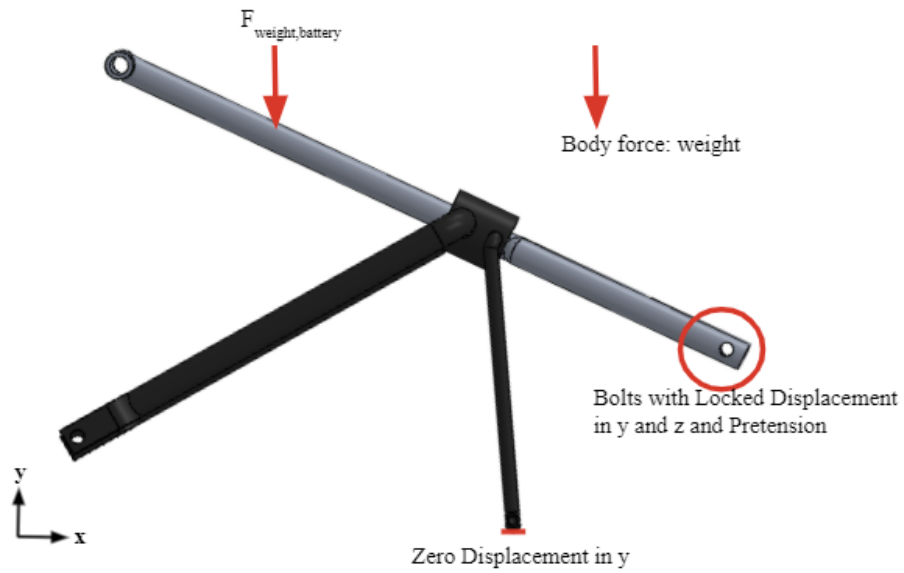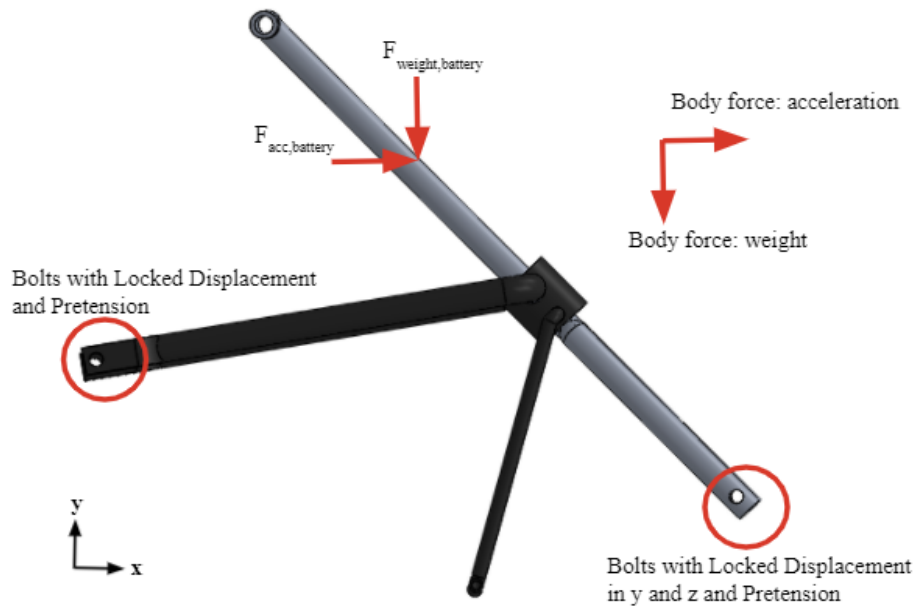
Figure 24: Loading Setup in Abaqus for (a) Disconnected from Wheelchair and (b) Connected to Wheelchair

The slightly overestimated values used for each load in the FEA can be found in Table 7 below.

Table 7: Magnitudes of Loads Applied in Abaqus Model

Load	Magnitude
Battery Weight	3.5 kg * 9.81 m/s^2 (~ 35 N)
Gravity	9.81 m/s^2
Acceleration	6 m/s/s or -6 m/s/s*
Pretension	1 kPa (on washer area)

*Based on the assumption that the vehicle accelerates to its maximum speed of 5.55 m/s (~ 6 m/s) in the interval of 1 second from rest.

Mesh

The meshing of the model was a critical phase owing to the irregular geometry and several numerical singularities such as re-entrant edges and concentrated forces. The re-entrant edges were resolved by making small fillets of 2 mm radius, while the concentrated forces were left as such.

Since the purpose of this FE model was to merely confirm the stresses in the chassis to be lower than yield stresses, no single specific area was of interest to us. Hence, the seeds for meshing were assigned globally and no partitions were made to the model for the sole purpose of meshing. Any edge or cell partitions produced were made to ease the application of loads and boundary conditions.

Owing to the involved model geometry, an unstructured mesh made of 3-dimensional continuum tetrahedron elements was produced. A quadratic nodal scheme for the elements was preferred over the linear scheme - the justification for which lies in the excessive

stiffness of the linear tetrahedron type owing to the rigidity of its sides which leads to an underestimation of the displacement field and an overestimation of the stress magnitudes [46]. Both the linear and quadratic elements can be seen in Fig 25 below. Abaqus refers to these linear 4-nodal tetrahedron elements as C3D4 and quadratic 10-nodal tetrahedron elements as C3D10 [46].
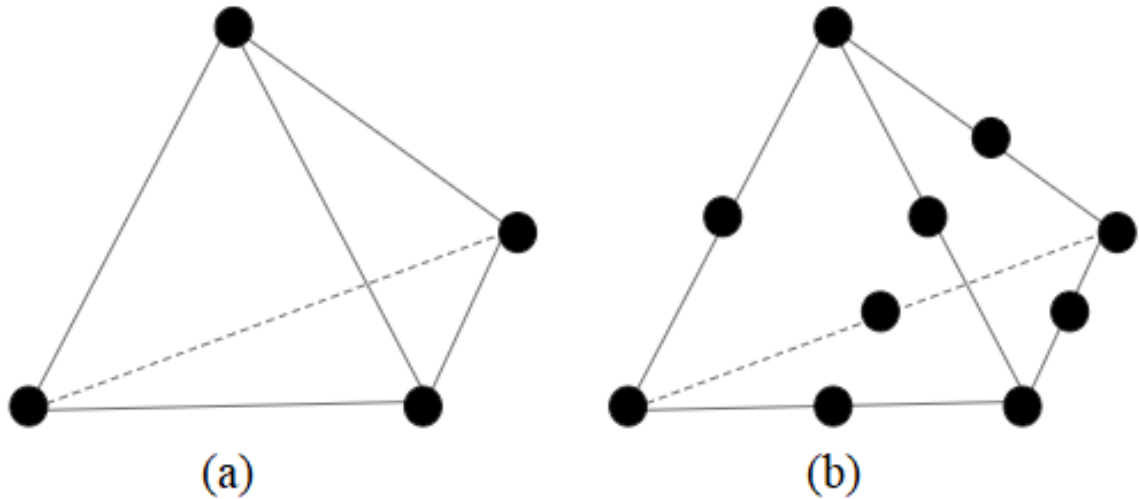
Figure 25: Abaqus Tetrahedron Elements (a) Linear C3D4 and (b) Quadratic C3D10

A simple mesh sensitivity study was performed on the static and disconnected case to verify convergence of the mesh using Maximum Von Mises stresses. The global seeds were reduced by 0.005 each step and the problem was solved with the new mesh while recording the Maximum Von Mises stresses. A plot between number of elements and Maximum Von Mises stresses can be seen in Fig 26 below followed by a 3D plot (Fig 27) between the same combined with Global Seeding data. The data for these plots can be found in *Appendix IV*.
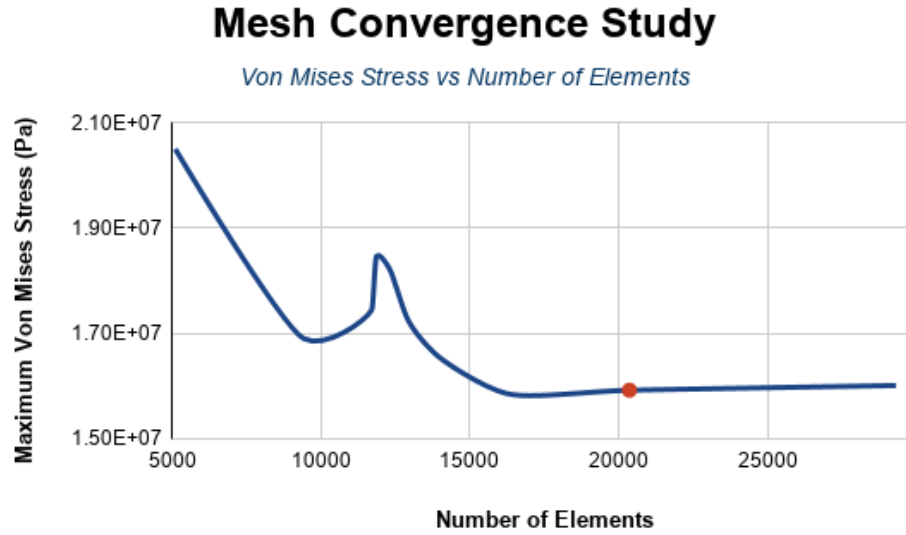
Figure 26: 2-Dimensional Plot between Maximum Von Mises Stresses and Number of Elements for Mesh Convergence Study
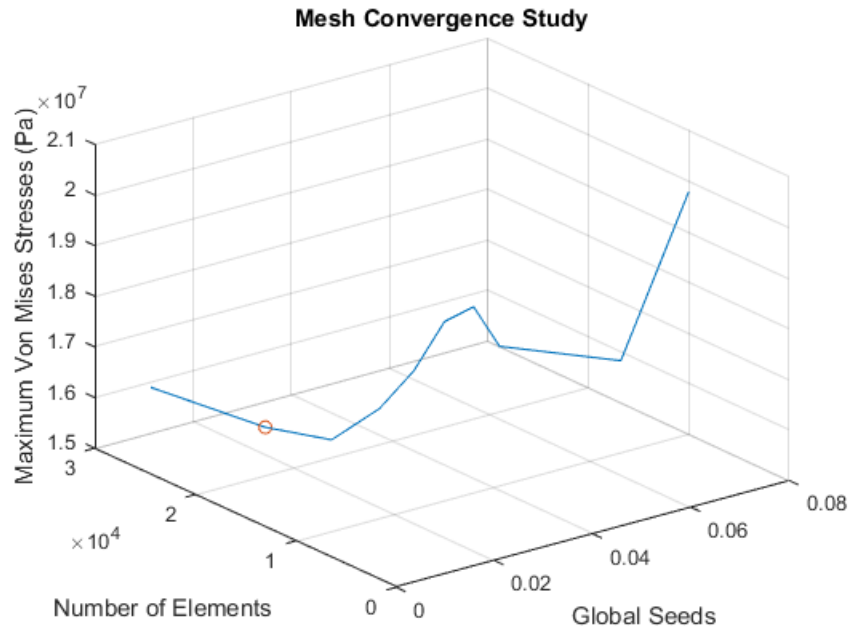
Figure 27: 3-Dimensional Plot between Maximum Von Mises Stresses, Number of Elements and Global Seeds

Some mesh properties can be found in the Table 8 below followed by the mesh itself in the Fig 28 below.

Table 8: Mesh Properties

Property	Value
Global Seeds	0.015
Number of Nodes	39566
Number of Elements	20392
Average Minimum Angle on Tri Faces	24.45º
Average Maximum Angle on Tri Faces	100.54º
Average Aspect Ratio	2.87
Average Geometric Deviation Factor	0.00133
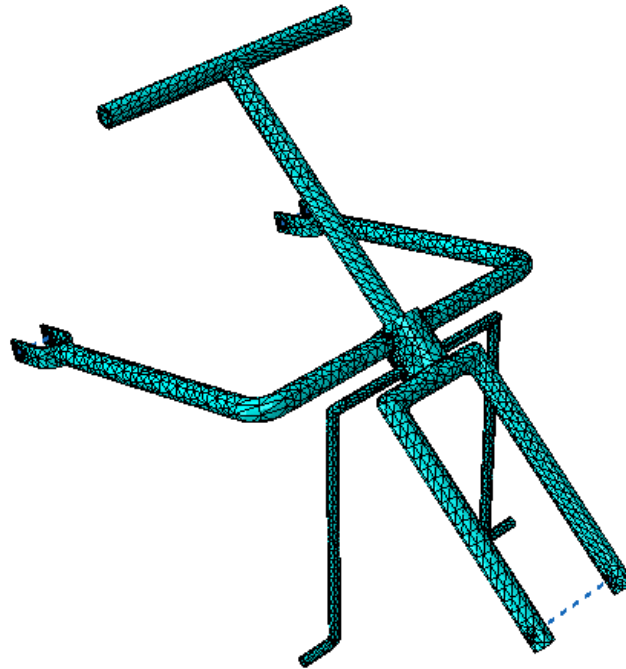
Figure 28: Unstructured Mesh of the Model using C3D10 Elements

Verification

In FEA, model verification is a major step to ensure that the software, essentially a black-box, does not churn out inaccurate results. To verify is to ascertain that the model was set up accurately and no errors were made while assigning properties or loads. A number of ways can be employed to verify the reliability of the values, some of which are shown in the following illustration named Fig 29.
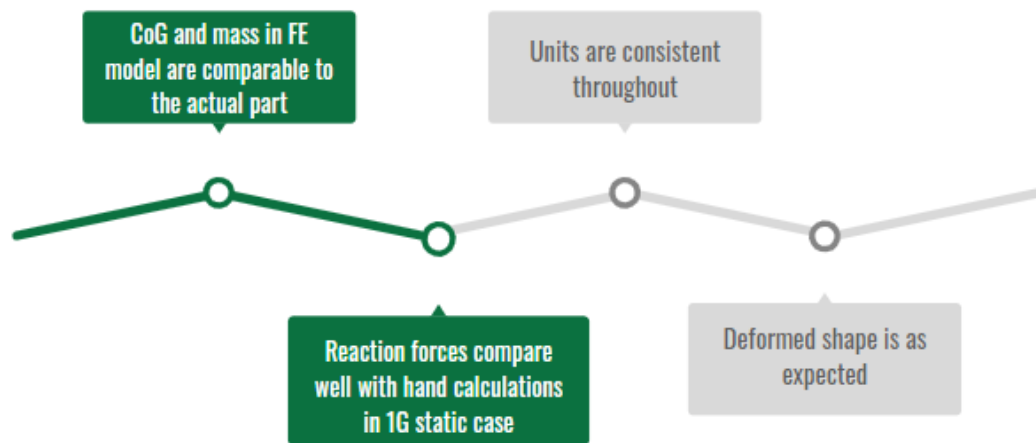
Figure 29: Possible Steps for Model Verification

As a first step of verification, it was ensured that all units have been consistently used against the SI system (kg, m, s). Then, the reliability of the deformed shape, with the single concentrated battery load, was ascertained, shown in Fig 30 below. Next, the CoG and mass of the model imported in Abaqus were compared to their counterparts in SolidWorks. Finally, the reaction forces from FE were compared with reactions from hand calculations, which can be found in *Appendix I*. This wrapped up the verification stage efficiently.
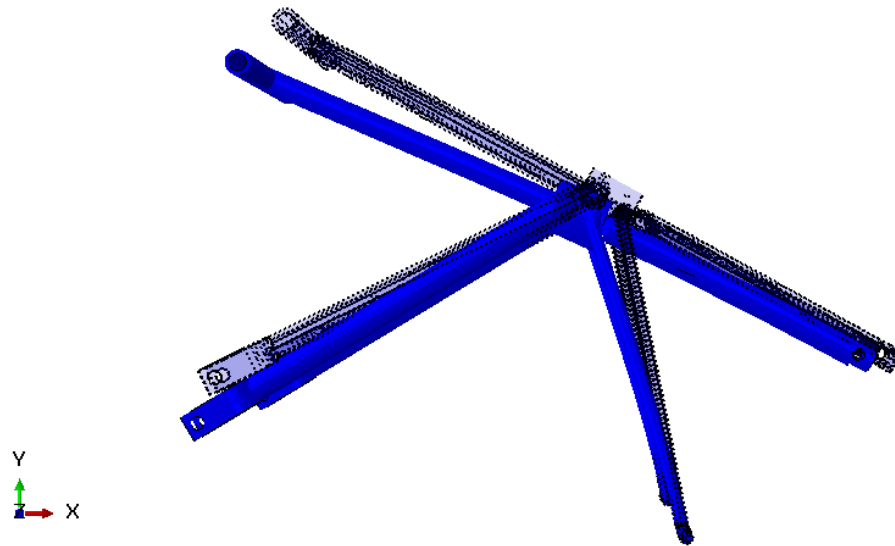
Figure 29: Deformed Shape of the Model under the Battery Load (scaled 50x)

Error Sources and Remedial Measures

As mentioned in Model and Material Parameters, the model was a simplified version of the real-world model and had a number of approximations and diminutions. Some of them have been listed below in Table 9 along with the steps taken for their remedy.

Table 9: Error Sources in the FE Model and Remedial Measures Taken

Error Source	Expected Effect on Results	Remedial Measure
Bolts modelled using connector elements	Lower accuracy in results	Bearing stresses in bolts calculated by hand using forces from FE results
Pretension stress assumed to be 1kPa	Stresses may be underestimated	Factor of Safety (FoS) should be able to compensate
Roller bearing modelled as a solid part	Stresses in bearing may be underestimated	Steel bearing with higher yield used instead of Aluminum bearing

Roller bearing and chassis modelled as single piece solid	Stresses due to interference fit will not be catered for	Stresses due to interference fit calculated separately by hand
Battery load (weight and acceleration) modelled as concentrated forces	Stresses may be overestimated locally	Saint-Venant's principle followed to ignore local stresses near a concentrated force

Analyses' Results

Detailed results of the analyses can be found in *Results and Discussion*. A summary of the results has been provided in the Table 10 below.

Table 10: Summary of FE Analyses' Results

Part	Maximum Von Mises Stress (MPa)	Factor of Safety
Steering Rod	198	1.4
Stand	15.92	17
Chassis	228	1.21
Bolts	0.3	920

Manufacturing

A simple and easy scheme has been devised for manufacturing and/or assembling the various parts of the power attachment. The manufacturing processes being used in this assembly can be divided into four types, shown in Fig 31 below.
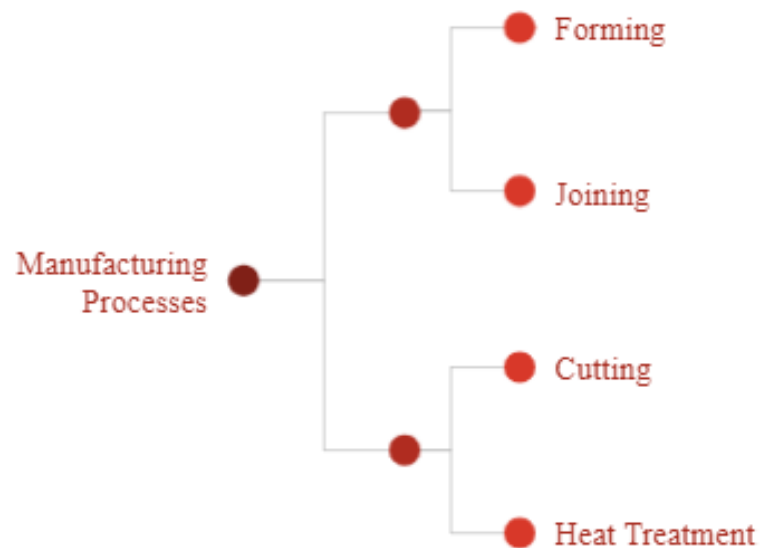
Figure 30: Manufacturing Processes Required

The forming processes include bending, shearing and turning (lathe), the joining processes include welding, bolting and press-fitting, the cutting processes include drilling and the heat treatment required is T6 (tempering). The manufacturing of each part from the raw material and assembling will be described in the coming paragraphs.

Chassis

The chassis (including kickstand), shown in Fig 20, is made using of four Aluminum 6061-T6 pipes, one Aluminum 6061-T6 sheet and one Aluminum 6061-T6 block. To manufacture it, we require two pipes of dimensions 30 mm x 674 mm and 30 mm x 674 mm with a thickness of 5 mm each, two pipes of dimensions 15 mm x 452 mm and thickness of minimum 2.5 mm, a sheet of dimensions 406 mm x 30 mm x 5 mm, and a block of dimensions 68 mm x 70 mm x 68 mm.

- Take the 30 mm x 674 mm pipes and cut both their ends to make round conical sections of radius 25 mm and 33.5 mm.

- At a distance of 241 mm from the 33.5 mm radius cut, bend both pipes at a 90°.
- Take the 68 mm x 70 mm x 68 mm block and using a lathe and turning operation, convert it into a cylinder of 67 mm x 70 mm. Then, using the lathe and drilling operations, hollow the cylinder to give an internal diameter of 62 mm.
- Take the 15 mm x 452 mm pipes and cut one end to make a round conical section of radius 33.5 mm.
- At a distance of 120 mm from the cut end, bend them at a 90°. At a distance of 32 mm from the other end, do the same.
- Take the 406 mm x 30 mm x 5 mm sheet, and cut it into two parts to get two identical pieces of 203 x 30 mm x 5 mm.
- Bend both the pieces at the center to give a diameter of 50 mm.
- Drill holes for an M15 bolt in both the arms of the bent sheets at a distance of 13 mm from the free ends. This finalizes the U-shaped clamps.
- Join the pipes to the cylinder (made from the block) and the U-shaped clamps using any welding technique suitable for Aluminum 6061 (say: MIG or pulsed-MIG welding with a filler wire of Aluminum 5356).
- Treat the structure with heat to re-establish T6 tempering for restoring the strength lost due to welding.

Roller Bearing

Press-fit the roller bearing of outer diameter equal to 62 mm into the cylinder of the chassis.

Steering

The steering, shown in Fig 19, comprises of three Aluminum 6061-T6 pipes. To manufacture it, we require three pipes of dimensions 30 mm x 475 mm, 30 mm x 400 mm and 30 mm x 690 mm with a thickness of 5 mm each.

- Cut the first pipe on both ends into a round conical section of 15 mm radius to be able to fit second and third pipes into it.
- Press-fit it inside the roller bearing.

- Bend the third pipe at a 90º on both locations at a distance of 75 mm from its the center.
- Make holes to fit an M15 bolt on both legs of the third bent pipe, at a distance of 20 mm from the ends.
- Weld second and third pipe on first pipe using any welding technique suitable for Aluminum 6061 (say: MIG or pulsed-MIG welding with a filler wire of Aluminum 5356).
- Treat the structure at its welded portions with heat to re-establish T6 tempering for restoring the strength lost due to welding.

Assemble

- Bolt the hub motor tire (including the disc brakes) to the steering.
- Attach the handle grip and brake handle to the steering.
- Attach the battery housing (including the battery) to the steering.
- Make connections of the battery with motor and throttle, and attach the throttle to the steering.
- Connect the attachment to the wheelchair through bolts and nuts.

CHAPTER 4: RESULTS AND DISCUSSIONS

In this chapter, the reader will come across the results for all finite element as well as hand calculations, a factor of safety calculated in each case using Von Mises Failure Criterion of Ductile Materials, the final design of the attachment, the selections for each component made and recommendations for where to easily buy them, specifications of the attachment produced in comparison with the objectives set while initiating the project along with a comparison of the same with the products available in the market, a basic cost analysis of the attachment, and finally a discussion on the safety measures and protocols.

Final Design and Dimensions

Using the results obtained from the analyses, material reduction wherever beneficial and taking into account the manufacturing processes, the final product design was established as shown in Fig 32.

(a)

(b)

Figure 31: CAD Model of the Final Design (a) without wheelchair (b) with wheelchair

The manufacturing drawings of the various parts can be found in *Appendix V*.

Final Component Selection

Final component selections keeping in mind the manufacturing processes described have been provided in Table 11.

Table 11: Final Selections of Components for the Attachment based on Availablility

Component	Selection
Structure	Aluminum 6061-T6 pipes
	Aluminum 6061-T6 sheet
	Aluminum 6061-T6 block
Roller Bearing	NU 206
Hub Motor	36 V, 250 W, 400 RPM
Tire	13x5-6, Vacuum Tubeless
Brakes	Disc
Throttle	Thumb/Twist, 36V
Battery	36 V, Lithium ion, 8 Ah
Bolts	M15, Aluminum
Nuts	M15, Aluminum
Washers	M15, Aluminum

Results of Analyses

As mentioned earlier, four different analyses were carried out on the simplified CAD model of the chassis and the von mises stresses were recorded for each. The following sections display the stress results along with the safety factor in each case. The FoS in each case has been calculated using Eq (2):

$$FoS = {\sigma_y}/{\sigma_{mises}} \qquad (2)$$

Disconnected from Wheelchair: Static

This case represents the attachment when it is not connected to the wheelchair. It stands supported through the kickstand on one end and the tire assembly pushing down on it on the other end. Both ends have been constrained through zero displacement boundary conditions, and a concentrated force of 35 N to represent the battery's weight has been applied to a point on the steering pipe. The von mises stress results can be seen in Fig 33 below, while Table 12 shows the maximum stresses in the different parts for this case.

Figure 32: Von Mises Stress Contours for Case 1: Static, Disconnected from Wheelchair

Table 12: Von Mises Stress Results for Case 1: Static, Disconnected from Wheelchair

Part	Von Mises Maximum Stress (MPa)	Factor of Safety
Steering	15.92	17
Chassis	0.5634	490
Stand	15.92	17

Connected to Wheelchair: Static

This case represents the attachment when it is connected to the wheelchair but static. It stands supported through the wheelchair on one end and the tyre assembly pushing down on it on the other end. Both ends have been constrained through zero displacement boundary conditions and bolt pretension has been applied in the form of pressure, with a concentrated force of 35 N to represent the battery's weight. The von mises stress results can be seen in Fig 34 below, while Table 13 shows the maximum stresses in the different parts for this case.

Figure 33: Von Mises Stress Contours for Case 2: Static, Connected to Wheelchair

Table 13: Von Mises Stress Results for Case 2: Static, Connected to Wheelchair

Part	Von Mises Maximum Stress (MPa)	Factor of Safety
Steering	10.82	25.5
Chassis	10.82	25.5
Stand	0.6645	415

Connected to Wheelchair: Accelerating

This case represents the attachment when it is connected to the wheelchair and accelerating forward. It is supported through the wheelchair on one end and the tyre assembly pushing down on it on the other end. Both ends have been constrained through zero displacement boundary conditions and bolt pretension has been applied in the form of pressure, with a concentrated force of 35 N to represent the battery's weight. The structure and the battery have been assigned an acceleration of 6 m/s^2 for forward accelerative forces. The von mises stress results can be seen in Fig 35 below, while Table 14 shows the maximum stresses in the different parts for this case.
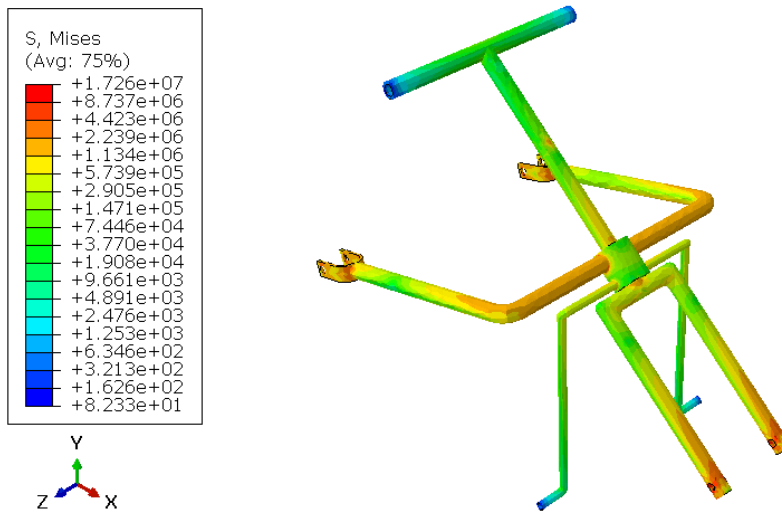
Figure 34: Von Mises Stress Contours for Case 3: Accelerating, Connected to Wheelchair

Table 14: Von Mises Stress Results for Case 3: Accelerating, Connected to Wheelchair

Part	Von Mises Maximum Stress (MPa)	Factor of Safety
Steering	17.26	16
Chassis	17.26	16
Stand	1.134	243

Connected to Wheelchair: Decelerating

This case represents the attachment when it is connected to the wheelchair and accelerating backward (decelerating). It is supported through the wheelchair on one end and the tire assembly pushing down on it on the other end. Both ends have been constrained through zero displacement boundary conditions and bolt pretension has been applied in the form of pressure, with a concentrated force of 35 N to represent the battery's weight. The structure and the battery have been assigned an acceleration of -6 m/s^2 for backward accelerative forces. The von mises stress results can be seen in Fig 36 below, while Table 15 shows the maximum stresses in the different parts for this case.

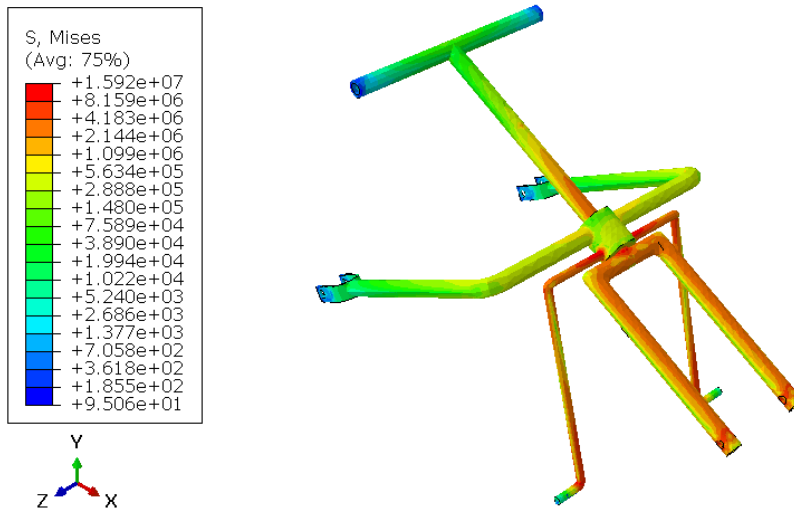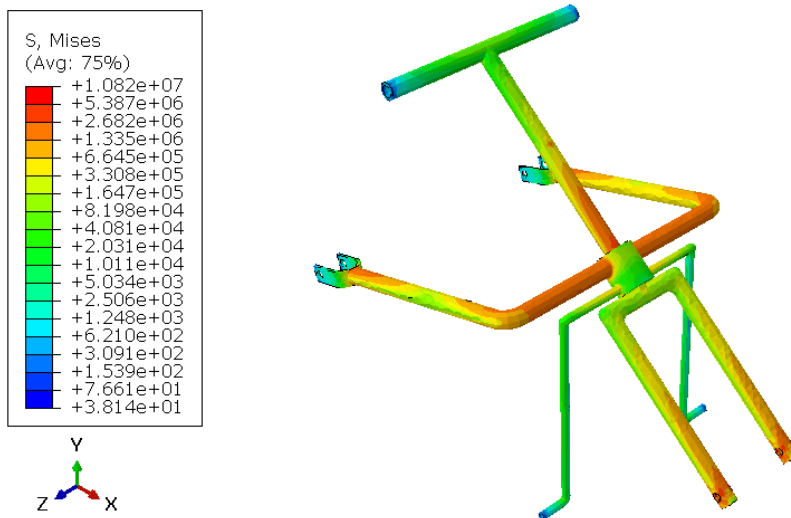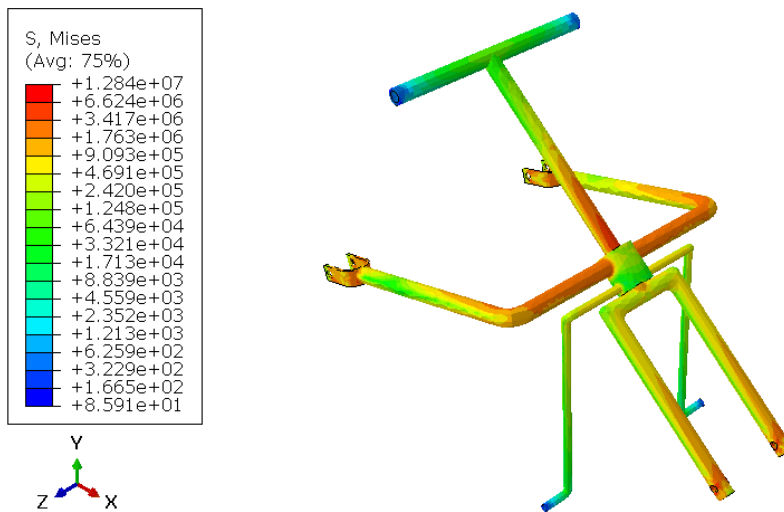Figure 35: Von Mises Stress Contours for Case 4: Decelerating, Connected to Wheelchair

Table 15: Von Mises Stress Results for Case 4: Decelerating, Connected to Wheelchair

Part	Von Mises Maximum Stress (MPa)	Factor of Safety
Steering	12.84	21
Chassis	12.84	21
Stand	1.763	156.6

Stresses in Bolts

The bearing stresses in the bolts were calculated by hand. Only stresses in one bolt were calculated, given the symmetrical geometry and loading conditions. However, the calculations for the motor shaft were not made as it cannot be changed or reinforced. Table 16 below shows the bearing stresses in each case with the factor of safety. The calculations can be found in *Appendix I*.

Table 16: Stresses in Bolts

Case	Bearing Stress (MPa)	Factor of Safety
Static, Disconnected	0	-
Static, Connected	0	-
Accelerating, Connected	0.3	920
Decelerating, Connected	0	-

Stresses due to Interference Fit of Roller Bearing

The Roller bearing, steering pipe and chassis assembly was connected through interference fits on both sides, as discussed in Manufacturing. The stresses due to interference were calculated and can be found in the Table 17 below.

Table 17: Stresses due to Interference Fit

	Stress (MPa)	Factor of Safety
Bearing, Steering	198	1.4
Chassis, Bearing	228	1.21

Cost Analysis of the Product

A cost breakdown of the product manufactured as a prototype has been provided in the Table 18 below, inclusive of taxes according to the Customs Act of 1969 by Government

of Pakistan [47] applied on products imported from other countries. USD to PKR conversion was made according to Eq (1-a).

Table 18: Cost Analysis of a Prototype for the Attachment

Item	Cost (PKR)	Shipping	Cost after Tax (PKR)	Quantity	Total
Aluminum	400 [20]	0	400	5	2000
Hub Motor Tire with Disc Brakes	12920 [48]	836*	18222.21554	1	18222.21554
Bearings	1895 [49]	0	1895	1	1895
Bolts, nuts, washers	300	0	300	1	300
Battery + Housing	7448 [50]	532*	10888.02548	1	10888.02548
Throttle	1785 [51]	0	1785	1	1785
Manufacturing	2090	0	2090	1	2050
Total Cost					**~37180**

*Shipping cost calculated at a rate of 1 USD per kg [52].

A detailed cost analysis with imposed taxes can be found in *Appendix VI*.

Specifications of the Final Model

Major specifications of the final model produced, such as weight, top speed, range, et cetera, have been listed in the Table 19 below.

Table 19: Specifications of the Final Model

Property	Value
Weight (kg)	~ 16

Max Speed (kmh)	20
Max Acceleration (m/s²)	6
Range (km)	35
Cost (PKR)	37180

Comparison with Major Market Contenders

To give an overview of the pros and cons of this product, Table 20 shown below has been constructed for a summarized comparison between this product and major market contenders. The products chosen for comparison can be found in *Available Designs*.

Table 20: Comparison of the Product with Major Market Contenders *[8-16]*

	Max Speed (km/h)	Range per Charge (km)*	Cost (PKR)**	Portability	Ease of Attachment
Our Product	20	35	~ 40,000	Yes	Yes
Firefly	19.3	15	~ 570,000	Yes	Yes
SmartDrive	10	5	~ 1,390,000	Yes	No
Mini-2	25	30	~ 1,523,000	Yes	Yes
Pride Jazzy	6.43	27.4	~ 843,000	No	N/A

Attachment by B.E. Appliances	20	30	~ 91,000	Yes	Yes

*Range calculated for maximum speed.

**Cost converted from USD to PKR according to Eq (1).

The comparison places the product at a reasonable competitiveness with a high range and a low cost as its key features. The graph below, shown in Fig 37, aims to provide an overall view of where our product lies in terms of cost, range and maximum speed possible.
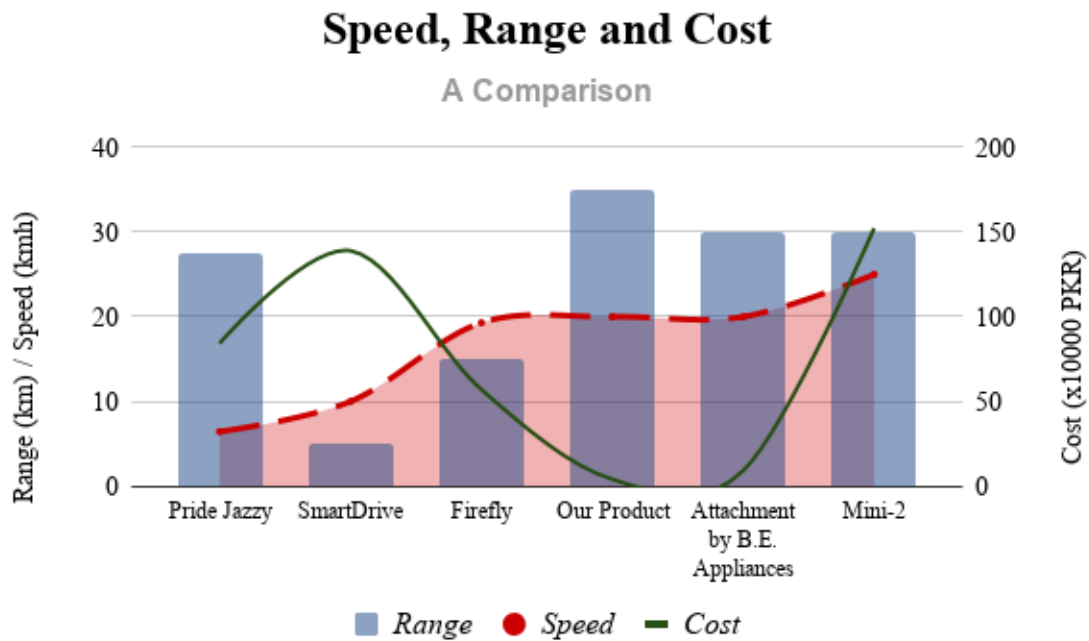
Figure 36: A Comparison of the Different Products in terms of Cost, Speed and Range

CHAPTER 5: CONCLUSION AND RECOMMENDATION

Finally, we conclude the project with some future recommendations. To summarize, the team accomplished all deliverables associated with the project. A literature review, the concept design, computer aided modelling, calculations and analysis were completed rigorously to achieve the goal of producing a cost-effective electric attachment for propelling a manual wheelchair.

From this chapter, the reader should expect a summary of the steps taken for project completion from start to end, a reiteration of the initial project objectives placed side-by-side with the goals achieved in the project, the potential this specific model holds, some future recommendations to be incorporated into projects of a similar standing, and link to an online repository which holds the CAD and FEA models for this project.

Summary of the Project

The project, based on the sole motivation of producing a cost-efficient design, was initiated with the demarcation of all deliverables which should be presented at the end of the project. The deliverables included, in broad terms

1. The concept design of the model with an easy mode of attachment to the wheelchair.

2. The CAD model of the design using SolidWorks.

3. A structural and dynamic analysis of the model using Abaqus CAE, and hand calculations wherever required.

4. A detailed manufacturing process along with the drawings.

All the deliverables have been included in this thesis.

The project execution began with a thorough literature review. This literature review involved a market survey of the products available which fulfill the same purpose, and a selection of the basic components for the model after weighing pros and cons of the easily available parts.

The next step was to prepare an initial design concept and produce a CAD model. This model was then put through a careful FEA analysis which turned the modelling process into an iterative one whereby material (thereby cost) reduction was meticulously judged against the induced stresses under harsh loading conditions. In this process, detailed hand calculations were also performed to judge the stresses in certain parts. This thesis only encloses the calculations for the final model. To conclude, the design underwent precise calculations and was judged against various factors such as cost, weight, stresses, ease of utilization etc.

Once the design was completed, the team moved onto the phase of deciding an easy and cheap manufacturing process for the product. Easily manageable and cheap processes such as welding, bolting and turning were utilized to finalize the product. It was also decided that certain parts would require heat treatment, specifically tempering, to gain their material strength once welded.

In the final phase, a detailed cost analysis was produced along with the various drawings of the product to assist the reader and/or future innovators. The following Fig 38 is a sharp indicator of the time spent on the various phases with respect to the cumulative time while working on this project.
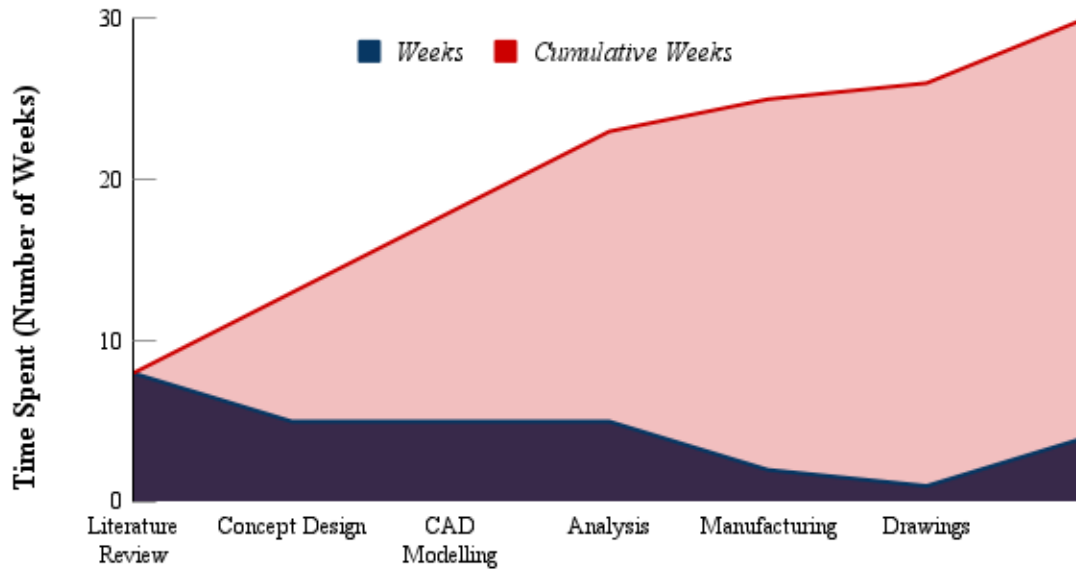
Figure 37: Time Required to Complete Various Phases Relative to the Cumulative Time Spent on the Project

Specifications of the Product Compared to Initial Objectives

As a final exercise, the specifications of the ultimate product have been judged against the initial objectives posed for the project. This data can be found in the Table 21 below.

Table 21: Comparison of Project Objectives with the Final Model

Feature	Objective	End Product
Cost	Minimize the cost to less than PKR 50,000.	PKR 37,180
Speed	Provide a minimum speed of 15 km/h which can be controlled.	20 km/h
Range	Provide a minimum range of 20 km to minimize charging frequency.	35 km

Weight/Portability	Minimize the attachment weight to less than 25 kg.	16 kg

A quick analysis of the table shows the product is successful and able to meet all minimum demands set initially.

Potential Improvements to the Product

From the numerous available products in the market [2-8], it is evident that the field of electrical wheelchairs is wide and deep, hence, it is clear that designing an attachment has several aspects to it which have not been considered during this project due to the paucity of time and resources. Therefore, this section aims to enlist changes and/or additions to the design, modelling, analysis and manufacturing phases which can be incorporated in the project by an eager innovator in the future to come.

Material Reduction

During our discussion in the section on results (see *Results and Discussion*), it was shown that the Factor of Safety (FoS) in most regions of the attachment, away from the interference fit, is higher than required for this scenario. Since the manufacturing process takes raw material in the form of uniform cross-sectioned pipes, it is unwise to reduce the material in areas away from the bearing for the sake of weight reduction, as it will add significant complexity to the manufacturing phase – hence, some material reduction in the model was ignored even though possible. However, all future designers are urged to ruminate over possible material reduction schemes which do not complicate the manufacturing process or become a loss financially.

Cheaper Alternatives to Off-the-Shelf Components

As witnessed in the section on components (see *Design Components*), a number of off-the-shelf components were borrowed as they were to assemble the final product. Some of these components were throttle, disc brakes, hub motor tire and battery housing. In all likelihood, it is possible to replace at least some of these components with cheaper alternatives, one example of which has been presented in *Appendix III* by replacing a throttle with a

potentiometer, reducing the cost by an 80%. Other possible changes include self-designing a cheap battery housing and observing the feasibility of rim brakes instead of disc brakes. It might also be possible, in a different design, to separate the motor and the tire and take cheaper local alternatives to both of them, given that nearly 35% of cost is added to the hub motor tire due to levied import taxes.

Suspension

For this project, it was decided to not include a suspension in the design due to the relatively low speed magnitude. However, the user may still experience small to moderate jumps while moving over speed breakers, potholes and other similar features. It is recommended for future that suspensions be looked into and modelled keeping in mind the fundamentals of mechanical vibrations.

Green Power Sources

The authors feel the need to emphasize that green (renewable) energy should be researched and looked into for the purpose of powering electrical wheelchairs. The easiest green source to incorporate in this domain would be solar energy. Designs which enable the placement of a solar panel have been considered before [53-55] and should be researched and prioritized over other power sources.

Analysis Improvements

In the section pertaining to the FEA analysis, a detailed table was provided which included several approximations made in the FE model (see *Error Sources and Remedial Measures*). For future, it is recommended to perform an in-depth FE analysis by using a model closer to the real model, if computational power available allows for it. This means:

1. Importing the CAD model of the bearing from the manufacturer and designing a contact analysis between the bearing and the other parts.
2. Replacing the concentrated force owing to the battery with a solid model of the battery housing containing the battery – also a contact analysis.

3. Modelling solid bolts instead of connectors.

Further, in the future, the design can also be put to test with a fatigue and fracture analysis since the material used has no endurance limit. Similarly, since it is possible for the final invalid carriage to become a subject of collision or impact with a high speed vehicle, the design should also be tested for crash and impact.

Online Repository for Models

For assistance of keen innovators in the future, an online repository has been established. The folder contains all the files of the assembly including all its parts. It also contains the input files for all four cases the attachment was tested against. The repository can be accessed through the following link:

https://drive.google.com/drive/folders/1-gT-d3NH_qDLgLxGrTPIcMcCpVNa8rBv?usp=sharing

REFERENCES

[1]   Alibaba. (2021). Retrieved 1 May 2021, from https://www.alibaba.com/

[2]   Batec Mobility - Add-on handbikes for wheelchair: manual and power handbikes easy to attach to the wheelchair. Revolutionary anchoring system - Batec Mobility. (2021). Retrieved 1 May 2021, from https://batec-mobility.com/en/

[3]   Rio Mobility - Turn your wheelchair into a power scooter. (2021). Retrieved 1 May 2021, from https://riomobility.com/

[4]   Permobil. (2021). Retrieved 1 May 2021, from https://www.permobil.com/en-gb

[5]   Corp., P. (2021). Pride Mobility® | Live Your Best® - Leader In Mobility Solutions. Retrieved 1 May 2021, from https://www.pridemobility.com/

[6]   Alltrack M3 Power Wheelchair - AMI Mobility. (2021). Retrieved 23 May 2021, from https://amimobility.com/shop/brands/alltrack-m3-power-wheelchair/

[7]   Wheelchair Power Attachment. (2021). Retrieved 23 May 2021, from https://www.hurt-e.cz/en

[8]   Cheapest Electric Wheelchair Handcycle Attachment 500w Wheel Size For Manual Wheelchair - Buy Electric Wheelchair,Electric Wheelchair Handcycle,Cheapest Electric Wheelchair Product on Alibaba.com. (2021). Retrieved 23 May 2021, from https://www.alibaba.com/product-detail/Cheapest-electric-wheelchair-handcycle-attachment-500w_1600080957081.html?spm=a2700.details.0.0.592174c43XAPJ9

[9]   Firefly. (2021). Retrieved 23 May 2021, from https://cdn.shopify.com/s/files/1/0156/5084/8816/files/Firefly_2.5_Sales_Sheet_sm_sz.pdf?v=1607467215

[10] Rio Mobility Firefly 2.5 Electric Handcycle. (2021). Retrieved 23 May 2021, from https://www.1800wheelchair.com/product/rio-mobility-firefly-electric-handcycle/

[11] SmartDrive. (2021). Retrieved 23 May 2021, from https://permobilwebcdn.azureedge.net/media/45ni04kz/smartdrive-pushtracker-e2-data-sheet.pdf

[12] SmartDrive MX2+ Power Assist by Max Mobility. (2021). Retrieved 23 May 2021, from https://www.sportaid.com/smartdrive-power-assist-by-max-mobility.html

[13] S.L., B. (2021). BATEC MINI 2, the minimum expression of Batec, the maximum expression of you. Retrieved 23 May 2021, from https://batec-mobility.com/en/products/handbikes/batec-mini-2-en

[14] Batec Mobility. (2021). Retrieved 23 May 2021, from https://www.49bespoke.com/index.php/online-store/31/batec-power

[15] ES, J. (2021). Jazzy 600 ES. Retrieved 23 May 2021, from https://www.pride-mobility.co.uk/jazzy-power-chairs/jazzy-600es.html

[16] Pride Jazzy. (2021). Pride Jazzy 600 ES Power Wheelchair – Limited Time Free White Glove Delivery - SpinLife. Retrieved 23 May 2021, from https://www.spinlife.com/Pride-Jazzy-600-ES-Full-Size-Power-Wheelchairs/spec.cfm?productID=103386

[17] van Blommestein, C., Boyce, R., Cole, R., & Marks, M. (2019). *POWER–ASSIST WHEELCHAIR ATTACHMENT*. Santa Clara, California. Retrieved from https://scholarcommons.scu.edu/mech_senior/90/

[18] Callister, W., & Rethwisch, D. (2012). *Materials science and engineering* (8th ed.). Hoboken, New Jersey: John Wiley & Sons.

[19] (2021). Retrieved 17 December 2020, from http://www.paksteel.com.pk/price_list.html

[20] Noor Ashraf and Sons Traders | Metal Products Suppliers in Pakistan. (2021). Retrieved 23 May 2021, from http://naaspak.com/

[21] Titanium Alloy Sheet Metal. (2021). Retrieved 23 May 2021, from https://www.alibaba.com/product-detail/Tc4-titanium-alloy-sheet-metal-material_62082681899.html?spm=a2700.galleryofferlist.normal_offer.d_title.78 8b6df5nWMple&s=p

[22] Pultruded Carbon Fiber Rod. (2021). Retrieved 23 May 2021, from https://www.indiamart.com/proddetail/pultruded-carbon-fiber-rod-22654063348.html

[23] Özdemir, N. (2005). Investigation of the mechanical properties of friction-welded joints between AISI 304L and AISI 4340 steel as a function rotational speed. *Materials Letters*, *59*(19-20), 2504-2509. doi: 10.1016/j.matlet.2005.03.034

[24] Zhang, J., Shen, Y., Li, B., Xu, H., Yao, X., Kuang, B., & Gao, J. (2014). Numerical simulation and experimental investigation on friction stir welding of 6061-T6 aluminum alloy. *Materials & Design*, *60*, 94-101. doi: 10.1016/j.matdes.2014.03.043

[25] Li, P., Nie, F., Dong, H., Li, S., Yang, G., & Zhang, H. (2018). Pulse MIG Welding of 6061-T6/A356-T6 Aluminum Alloy Dissimilar T-joint. *Journal Of Materials Engineering And Performance*, *27*(9), 4760-4769. doi: 10.1007/s11665-018-3528-y

[26] Atieh, A., Rawashdeh, N., & AlHazaa, A. (2018). Evaluation of Surface Roughness by Image Processing of a Shot-Peened, TIG-Welded Aluminum 6061-T6 Alloy: An Experimental Case Study. *Materials*, *11*(5), 771. doi: 10.3390/ma11050771

[27] Zhang, Y., Huang, J., Ye, Z., & Cheng, Z. (2017). An investigation on butt joints of Ti6Al4V and 5A06 using MIG/TIG double-side arc welding-brazing. *Journal Of Manufacturing Processes*, *27*, 221-225. doi: 10.1016/j.jmapro.2017.05.010

[28] Akman, E., Demir, A., Canel, T., & Sınmazçelik, T. (2009). Laser welding of Ti6Al4V titanium alloys. *Journal Of Materials Processing Technology*, *209*(8), 3705-3713. doi: 10.1016/j.jmatprotec.2008.08.026

[29] Turner, R., Gebelin, J., Ward, R., & Reed, R. (2011). Linear friction welding of Ti–6Al–4V: Modelling and validation. *Acta Materialia*, *59*(10), 3792-3803. doi: 10.1016/j.actamat.2011.02.028

[30] Striebel, K., Shim, J., Cairns, E., Kostecki, R., Lee, Y., & Reimer, J. et al. (2004). Diagnostic Analysis of Electrodes from High-Power Lithium-Ion Cells Cycled under Different Conditions. *Journal Of The Electrochemical Society*, *151*(6), A857. doi: 10.1149/1.1710514

[31] RC Lipo Battery Guide: Explanation, Safety, and Care • LearningRC. (2021). Retrieved 19 Dec 2020, from http://learningrc.com/lipo-battery/

[32] Omar, N., Monem, M., Firouz, Y., Salminen, J., Smekens, J., & Hegazy, O. et al. (2014). Lithium iron phosphate based battery – Assessment of the aging parameters and development of cycle life model. *Applied Energy*, *113*, 1575-1585. doi: 10.1016/j.apenergy.2013.09.003

[33] Lead-acid Rechargable Battery Information - Battery University. (2021). Retrieved 23 May 2021, from https://batteryuniversity.com/learn/archive/can_the_lead_acid_battery_compete_in_modern_times

[34] Li Ion 7.5ah Rechargeable Battery 36 V. (2021). Retrieved 23 May 2021, from https://www.alibaba.com/product-detail/New-design-li-ion-7-5ah_1600051368405.html?

[35] MaxAmps 36V 11Ah E-Bike LiPo Battery Pack. (2021). Retrieved 23 May 2021, from https://www.maxamps.com/36v-11ah-e-bike-lipo-battery-pack

[36] LiFePO4 36V Battery for Ebikes. (2021). Retrieved 23 May 2021, from https://www.amazon.com/BtrPower-Electric-1500W-350W-Tricycle-Motorcycle/dp/B07P5KQGW5?th=1

[37] Sealed Lead Acid Battery 12 V. (2021). Retrieved 23 May 2021, from https://www.amazon.com/Shock-dirt-Proofcases-Covers-Galaxy-S3/dp/B00QDBZUVO/ref=rtpb_1?pd_rd_w=GzBaR&pf_rd_p=be844577-fee7-4bbc-8dda-083e56cc6f0d&pf_rd_r=V857Q4Y2KE9EW43BCXP1&pd_rd_r=4e6d2d12-a215-4084-856a-7361b2d70566&pd_rd_wg=0Kr2T&pd_rd_i=B00QDBZUVO&psc=1

[38] Wang, Q., Sun, J., & Chu, G. (2021). Lithium Ion Battery Fire And Explosion. Retrieved 23 May 2021, from https://iafss.org/publications/fss/8/375/view/fss_8-375.pdf

[39] Baronti, F., Fantechi, G., Leonardi, E., Roncella, R., & Saletti, R. (2010). Enhanced model for Lithium-Polymer cells including temperature effects. *IECON 2010 - 36Th Annual Conference On IEEE Industrial Electronics Society*. doi: 10.1109/iecon.2010.5675134

[40] Summer, S., & Maloney, T. (2017). *Fire Hazard Analysis for Various Lithium Batteries*. New Jersey: U.S. Department of Transportation - Federal Aviation Administration. Retrieved from https://www.fire.tc.faa.gov/pdf/TC-16-17.pdf

[41] Parker, T., Obeng, L., & Wang, Q. (2020). *Fire Hazard Assessment of Lead-Acid Batteries*. College Station, Texas: Fire Protection Research Foundation. Retrieved from https://www.nfpa.org//-/media/Files/News-and-Research/Fire-statistics-and-reports/Hazardous-materials/RFLeadAcidBattery.pdf

[42] G. Delfin, M., & May G. Mendez, D. (2019). Ergonomic Design of an Assistive Propulsion System for Manual Wheelchairs. In *Proceedings of the International Conference on Industrial Engineering and Operations Management*. Intramuros, Manila: IEOM Society International.

[43] Singh, G., Singla, A., & S. Virk, G. (2016). Modeling and Simulation of a Passive Lower-Body Mechanism for Rehabilitation. In *Conference on Mechanical Engineering and Technology*.

[44] Budynas. (2020). *Shigley's Mechanical Engineering Design, 11th Edition, SI Units*. [S.l.]: Mcgraw-Hill Education

[45] Road bike disc brakes: everything you need to know. (2021). Retrieved 23 May 2021, from https://www.bikeradar.com/features/road-disc-brakes-everything-you-need-to-know/

[46] Selecting continuum elements. (2021). Retrieved 23 May 2021, from https://abaqus-docs.mit.edu/2017/English/SIMACAEGSARefMap/simagsa-c-ctmselecting.htm

[47] Federal Board of Revenue, Government of Pakistan. (2020). *Pakistan Customs Tariff-2020-21*. Islamabad: Printing & Publication Customs Budget FBR.

[48] 13 Inch 36v Motor With Tyre. (2021). Retrieved 23 May 2021, from https://www.alibaba.com/product-detail/13-inch-high-torque-36V-48V_62123995952.html?spm=a2700.galleryofferlist.normal_offer.d_title.3b9a3 b7e25obrr

[49] (2021). Retrieved 23 May 2021, from https://haspakistan.com

[50] Silver Fish 36v 8ah Lithium Battery For Ebike. (2021). Retrieved 23 May 2021, from https://www.alibaba.com/product-detail/36v-Lithium-36v-Original-Wholesale-Silver_1600178623624.html?spm=a2700.galleryofferlist.normal_offer.d_title.68 f735580tkaps&s=p

[51] Ebike Throttle. (2021). Retrieved 23 May 2021, from https://www.daraz.pk/products/ebike-throttle-48v-electric-bicycle-throttle-handle-accelerator-throttle-grip-electric-scooters-with-lock-i156888040.html

[52] Cheap Express Freight Forwarder Shipping Rates From China To Pakistan. (2021). Retrieved 23 May 2021, from https://www.alibaba.com/product-detail/cheap-express-freight-forwarder-shipping-rates_60773983327.html

[53] Takahashi, Y., & Matsuo, S. (2011). Running experiments of electric wheelchair powered by natural energies. *2011 IEEE International Symposium On Industrial Electronics*. doi: 10.1109/isie.2011.5984286

[54] Chien, C., Huang, T., Liao, T., Kuo, T., & Lee, T. (2021). Design and development of solar power-assisted manual/electric wheelchair. Retrieved 23 May 2021, from https://www.proquest.com/docview/1662444210?pq-origsite=gscholar&fromopenview=true

[55] Manohar Gurram, A., Ramana Rao, P., & Dontikurti, R. (2012). Solar Powered Wheel Chair: Mobility For Physically Challenged. INPRESSCO. Retrieved from http://inpressco.com/category/ijcet

[56] Mukherjee, D. (2014). Effect of Pavement Conditions on Rolling Resistance. American Journal of Engineering Research (AJER). Retrieved from http://www.ajer.org/papers/v3(7)/R037141148.pdf

[57] Princeton. *Drag coefficients of blunt and streamlined bodies* [Image]. Retrieved from https://www.princeton.edu/~asmits/Bicycle_web/pictures/drag_coeff_2.GIF

[58] Kosky, P. (2013). *Exploring Engineering* (3rd ed., pp. 259-281). Elsevier/AP.

[59] Amatya, R., & Ram, R. (2010). Solar Thermoelectric Generator for Micropower Applications. *Journal Of Electronic Materials*, *39*(9), 1735-1740. doi: 10.1007/s11664-010-1190-8

[60] Thermal Insulation of Plastics: Technical Properties. (2021). Retrieved 24 May 2021, from https://omnexus.specialchem.com/polymer-properties/properties/thermal-insulation

[61] Institute, E. (2021). Welder Arc Salary in Pakistan. Retrieved 24 May 2021, from https://www.erieri.com/salary/job/welder-arc/pakistan

[62] Institute, E. (2021). Salary Expert - Sheet Metal Cutter Metal Fabrication. Retrieved 24 May 2021, from https://www.salaryexpert.com/salary/job/sheet-metal-cutter-metal-fabrication/pakistan/karachi

[63] Institute, E. (2021). Salary Expert - Lathe Machinist Salary Pakistan. Retrieved 24 May 2021, from https://www.salaryexpert.com/salary/job/lathe-machinist/pakistan

[64] Item Duty Calculator. (2021). Retrieved 10 May 2021, from https://www.weboc.gov.pk/(S(tyorev0sgomt0ryf1n5rka13))/Shared/ItemGeneral DutyCalculator.aspx

APPENDIX I: DETAILED CALCULATIONS

Battery and Hub Motor Specifications

Data:

$$\text{Velocity} = v$$

$$v = 20 \ km/h \approx 5.55 \ m/s$$

$$\text{Air Density} = \rho_{air}$$

$$\rho_{air} = 1.226 \ kg/m^3$$

$$\text{Frontal Area} = A_f$$

$$A_f = 0.4 \ m * 1.13 \ m \approx 0.452 \ m^2$$

$$\text{Coefficient of Rolling Friction} = \mu \text{ (for rubber-asphalt)}$$

$$\mu = 0.013 \ [56]$$

$$\text{Total Mass} = m$$

$$m = \text{mass of average male} + \text{wheelchair} + \text{attachment}$$

$$m \approx 130 \ kg \ (= 80 + 30 + 20)$$

$$\text{Drag Coefficient} = C_d \text{ (for blunt structures)}$$

$$C_d = 1 \ [57]$$

$$\text{Required Range} = R$$

$$R = 35 \ km = 35000 \ m$$

$$\text{Voltage of battery/motor} = V$$

$$V = 36V \text{ (commonly available)}$$

$$\text{Motor Efficiency} = \emptyset$$

$$\emptyset = 90\% = 0.9 \text{ (assumed)}$$

$$\text{Motor Rotational Speed} = N$$

$$N \sim 400\ RPM$$

$$\text{Motor Speed} = \omega$$

$$\omega = 400 * \frac{2\pi}{60} \approx 41.88\ rad/s$$

Calculations:

$$\text{Drag Force} = \text{F}_d$$

$$\text{F}_d = 0.5 * C_d * \rho_{air} * A_f * v^2 \tag{3}$$

$$\text{F}_d = 8.55\ N$$

$$\text{Frictional Force} = f$$

$$f = \mu * m * g \tag{4}$$

$$f = 16.58\ N$$

$$\text{Total Tractive Force} = \text{F}$$

$$\text{F} = F_d + f \tag{5}$$

$$\text{F} = 25.13\ N$$

$$\text{Required Electric Power} = \text{P}_{elec}$$

$$\text{P}_{elec} = F * v \tag{6}$$

$$\text{P}_{elec} = 139.6\ W$$

$$\text{Required Battery Power} = \text{P}_{bat}$$

$$\text{P}_{bat} = \frac{\text{P}_{elec}}{\emptyset} \tag{7}$$

$$\text{P}_{bat} = 155.1\ W$$

$$\text{Energy Stored in Battery} = \text{E} = \frac{P_{bat} * R}{v} \tag{8}$$

$$E = 977130\ Ws = 271.425\ Wh$$

$$\text{Required Battery Capacity} = C_{bat}$$

$$C_{bat} = \frac{E}{V} \tag{9}$$

$$C_{bat} = 7.54\ Ah$$

$$\text{Tire Diameter} = \text{D}$$

$$\text{D} = \frac{2v}{\omega} \tag{10}$$

$$\text{D} = 0.265\ m \approx 11\ in$$

Final Battery Specifications:

36 V; 7.54 Ah; 155W

Lithium Ion Battery Surface Temperature Calculation

The following Fig 38 sets up an approximation for the heat transfer problem to find the surface temperature of the battery.
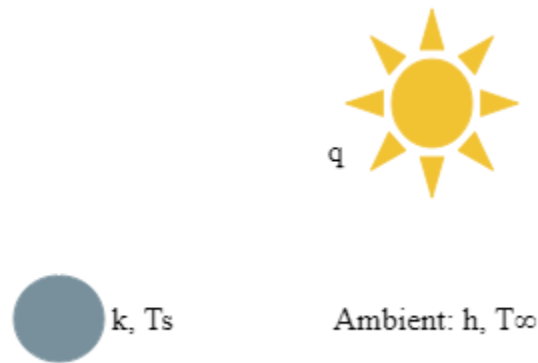

Figure 38: Setup of the Heat Transfer Problem for Battery Temperature

Assuming worst-case scenarios for each parameter,

$$\text{Convection Coefficient (free, air)} = h$$

$$h = 25\frac{W}{m^2K} \text{ [58]}$$

$$\text{Ambient Temperature} = T_\infty$$

$$T_\infty = 50 \text{ °C (assumed)}$$

$$\text{Solar Heat Flux} = q$$

$$q = 1000\frac{W}{m^2} \text{ [59]}$$

$$\text{Emissivity} = \varepsilon = 0.95 \ (assumed)$$

$$\text{Boltzmann's Constant} = \sigma$$

$$\sigma = 5.67 * 10^{-8}\frac{W}{m^2K^4}$$

Setting up the heat transfer equation as below:

$$q = \varepsilon\sigma(T_s^4 - T_\infty^4) + h(T_s - T_\infty) \tag{11}$$

$$T_s \approx 78.55\ °C$$

This values is higher than the explosion temperature of Li-ion batteries [38]. However, if this set of calculations are extended by assuming a planar plastic casing for the battery with a thickness of 1 cm, we can use the following equation between the battery and casing:

$$q = -\frac{k(T_b - T_s)}{t} \tag{12}$$

where:

$$k \le 0.5\frac{W}{m.K}\ \text{(plastic) [60]}$$

$$T_s = 78.55\ °C$$

$$\text{thickness} = t = 1\ cm = 1*10^{-2}m$$

$$q = 1000\frac{W}{m^2}$$

This gives a new surface temperature for the battery:

$$T_b = 58.55\ °C$$

This is lower than the battery explosion temperature. Therefore, this problem defines the base values for the battery housing.

Finite Element Model Verification Using Reaction Forces

 The static and disconnected load case was utilized to verify the setup of the FE model, as shown in Fig 39 below. The reaction forces in the y-direction at all nodes on the supporting legs were all summed up to give the total reaction force, which was compared with the total weight of the system.
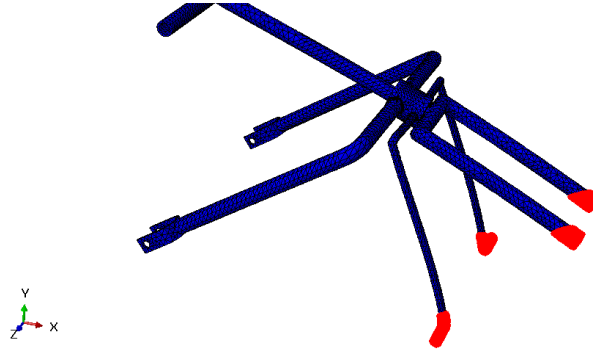

Figure 39: Nodes Used to Find the Total Reaction Force

Total Weight: Weight of Attachment + Weight of Battery

$$= (4.03745*9.81 \text{ N}) + (35 \text{ N})$$

$$\sim 75 \text{ N}$$

Total Reaction Force from FE at the end of step (shown in Fig 40 below): ~ 75 N
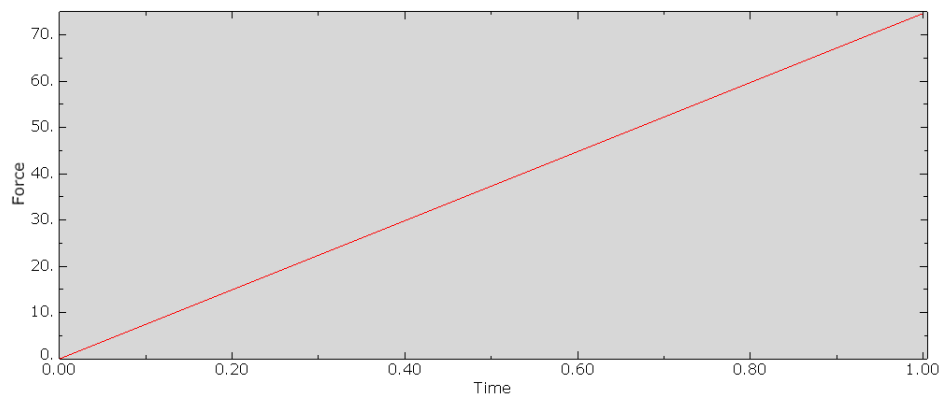

Figure 40: Total Reaction Force at the End of the Step

The two results conform to each other. This verifies the model setup.

Bearing Stresses in Bolts

For our bolts, the following apply:

$$\text{Radius of bolts} = r$$

$$r = \frac{15}{2}\, mm = 7.5 * 10^{-3} m$$

$$\text{Cross-sectional Area of bolts} = A$$

$$A = \pi r^2 \tag{13}$$

$$A = 1.7672 * 10^{-4} m^2$$

$$\text{Yield stress for Aluminum 6061-T6} = \sigma_y$$

$$\sigma_y = 276\, MPa\, [18]$$

Case 1: Static, Disconnected

No pulling force is acting on the bolt. The bearing stresses are, practically, zero.

Case 2: Static, Connected

No pulling force is acting on the bolt. The bearing stresses are, practically, zero.

Case 3: Accelerating, Connected

The forward accelerative forces pit the bolts against the wheelchair's arms leading to a 'pulling' effect which is similar to a double shear condition, as shown in Fig 41 below.
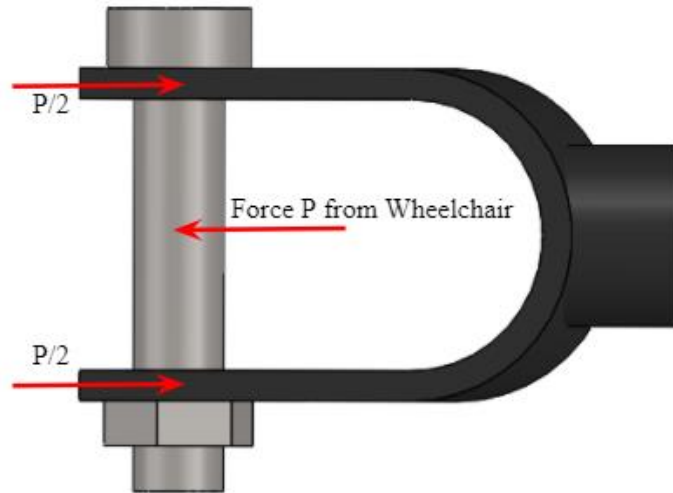
Figure 41: Double-shear Condition of the Bolt

The force in the arm pulling the bolt was taken from FE as shown in Fig 42 below:

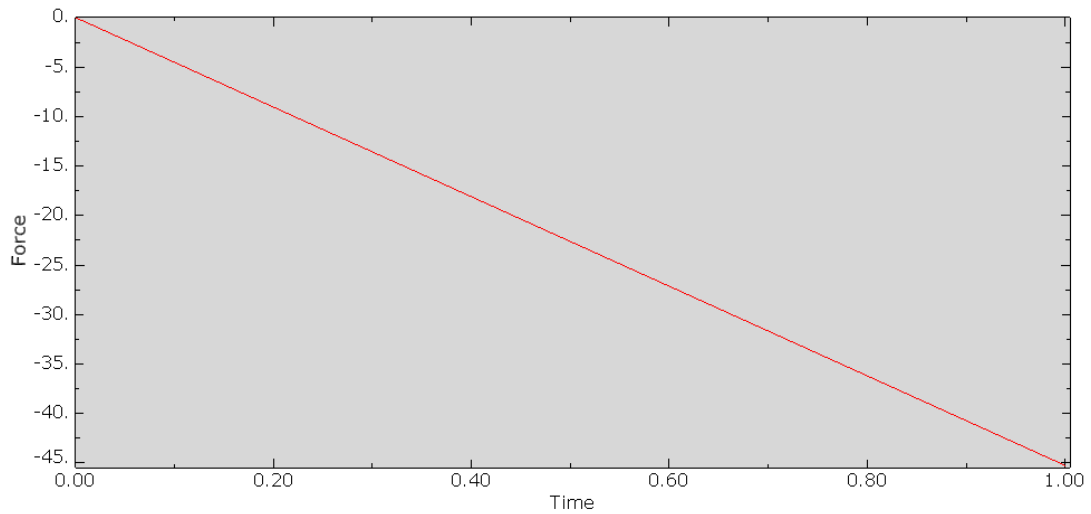$$\left|{}^{P}\!/_{2}\right| \approx 47.5 \ N$$

Figure 42: Force in the Clamp Arms at the End of the Step

The bearing stress in the bolt will then be:

$$\text{Average bearing stress} = \sigma_{b,avg}$$

$$\sigma_{b,avg} = {}^P\!/_{2A} \qquad\qquad (14)$$

$$\sigma_{b,avg} = 268787 \ Pa$$

$$\sigma_{b,avg} \approx 0.3 \ MPa$$

This leads to a high factor of safety of 920, and suggests that bolts need not be worried about.

Case 4: Decelerating, Connected

No pulling force is acting on the bolt. The bearing stresses are, practically, zero.

Stresses in Roller Bearing due to Interference Fit

The interference fit between the steering-bearing and bearing-chassis can be represented, simply, as the condition in Fig 43.
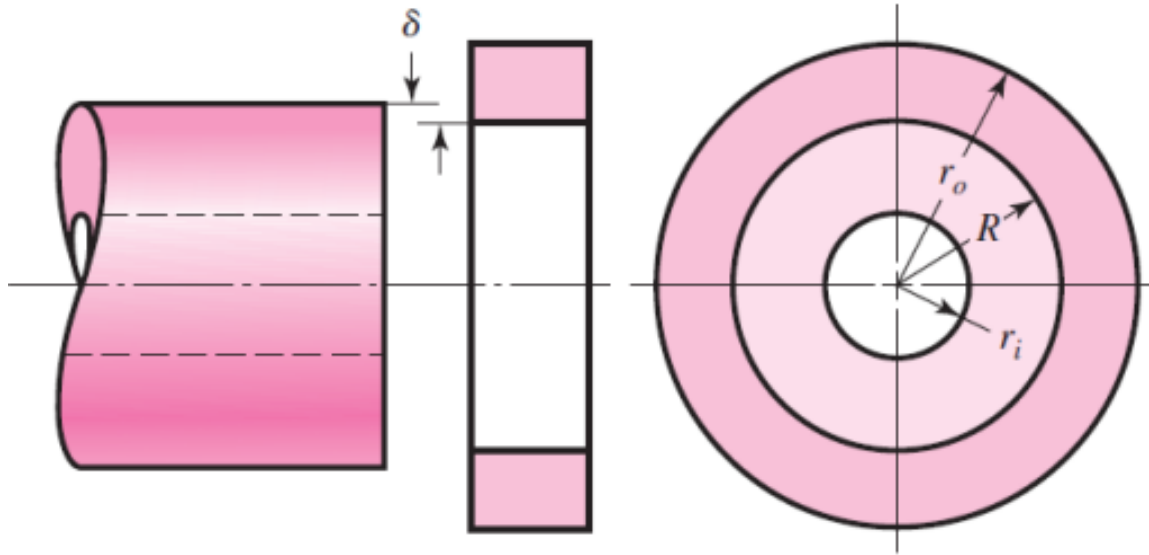

Figure 43: Interference Fit Nomenclature (taken from [44])

$$\text{Stress due to interference fit} = \sigma$$

$$\sigma = -\frac{\delta}{R\left[\frac{1}{E_o}\left(\frac{r_o^2 + R^2}{r_o^2 - R^2} + v_o\right) + \frac{1}{E_i}\left(\frac{R^2 + r_i^2}{R^2 - r_i^2} - v_o\right)\right]} \qquad (15)$$

Bearing-Steering:

$$\text{Interference} = \delta$$

$$\delta = 0.1 \; mm = 1 * 10^{-4} m$$

$$R = 0.01505 \; m$$

$$r_i = 0.0125 \; m$$

$$r_o = 0.031 \; m$$

$$E_i = 69.9 \, GPa$$

$$E_o = 210 \, GPa$$

$$v_i = 0.33$$

$$v_o = 0.3$$

$$\sigma_{y,i} = 276 \, MPa$$

$$\sigma_{y,o} = 320 \, MPa$$

$$\sigma = -198 \, MPa$$

$$FOS_o = abs(\sigma_{y,o}/\sigma)$$

$$FOS_o = 1.62$$

$$FOS_i = abs(\sigma_{y,i}/\sigma)$$

$$FOS_i = 1.4$$

Chassis-Bearing:

$$\delta = 1 \, mm = 1 * 10^{-3} m$$

$$R = 0.031 \, m$$

$$r_i = 0.015 \, m$$

$$r_o = 0.035 \, m$$

$$E_i = 210 \, GPa$$

$$E_o = 69 \, GPa$$

$$v_i = 0.3$$

$$v_o = 0.33$$

$$\sigma_{y,i} = 320 \, MPa$$

$$\sigma_{y,o} = 276 \; MPa$$

$$\sigma = -228 \; MPa$$

$$FOS_o = abs(^{\sigma_{y,o}}/_\sigma)$$

$$FOS_o = 1.21$$

$$FOS_i = abs(^{\sigma_{y,i}}/_\sigma)$$

$$FOS_i = 1.4$$

These FOS have been noted in the section *Results and Discussion*.

APPENDIX II: STANDARD PAKISTANI WHEELCHAIR DRAWING

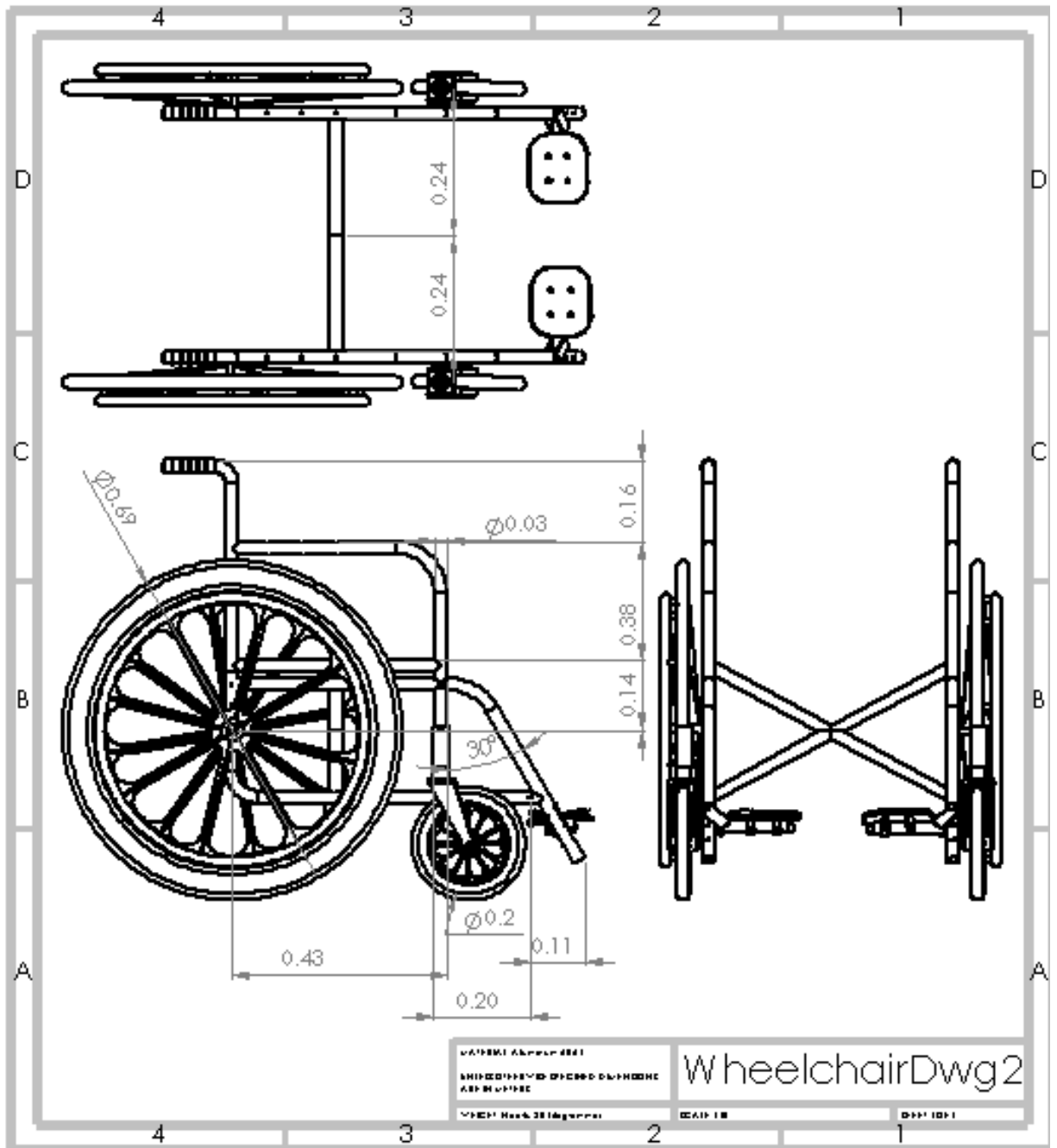Following Fig 44 gives the drawing for the standard wheelchair modelled.

Figure 44: Drawing of Standard Pakistani Wheelchair

APPENDIX III: ELECTRICAL CIRCUIT DIAGRAM

The following Fig 45 shows the electrical circuit which can be made by replacing the throttle with a potentiometer.
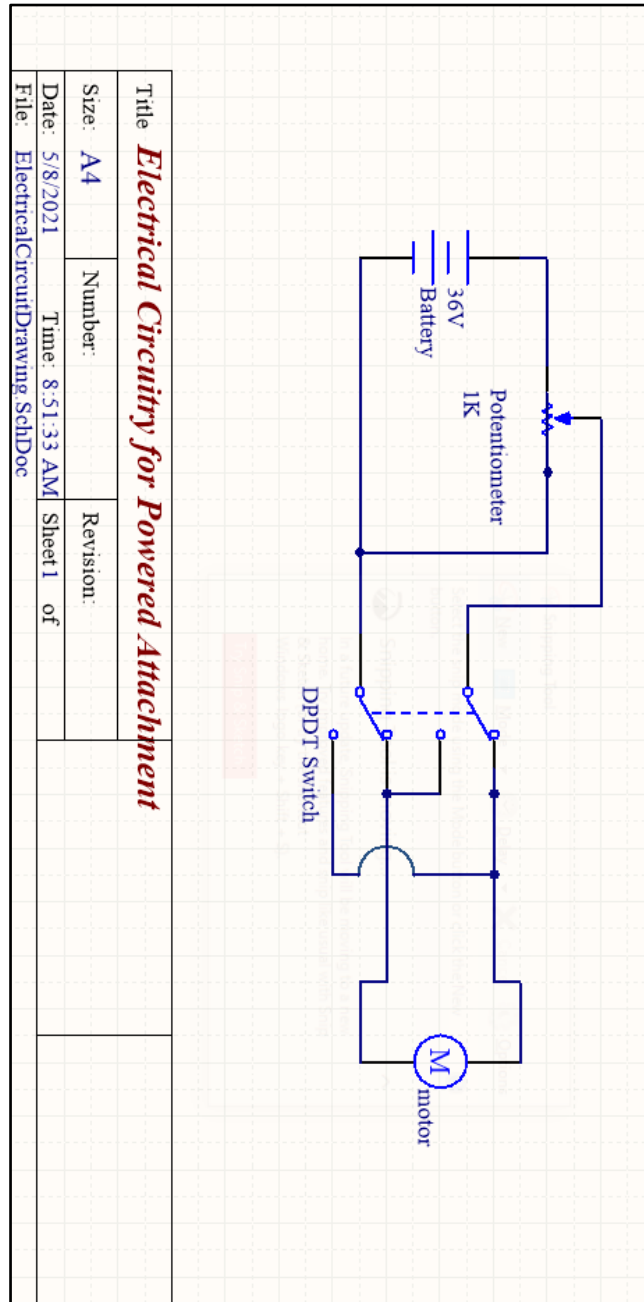

Figure 45: Electrical Circuit for the Attachment using a Potentiometer

APPENDIX IV: MESH CONVERGENCE STUDY DATA

The following data in Table 22 was accumulated from the various simulations run to for mesh convergence and forms the basis for Fig 26 and 27.

Table 22: Data used for Mesh Convergence Study Graphs

Global Seeding	Number of Elements	Maximum Von Mises Stress (Pa)
0.07	5108	2.05E+07
0.065	9420	1.69E+07
0.045	11718	1.75E+07
0.04	11851	1.84E+07
0.035	12298	1.82E+07
0.03	12921	1.73E+07
0.025	13882	1.66E+07
0.02	16214	1.59E+07
0.015	**20363**	**1.59E+07**
0.01	29318	1.60E+07

APPENDIX V: MANUFACTURING DRAWINGS

Chassis with Stand

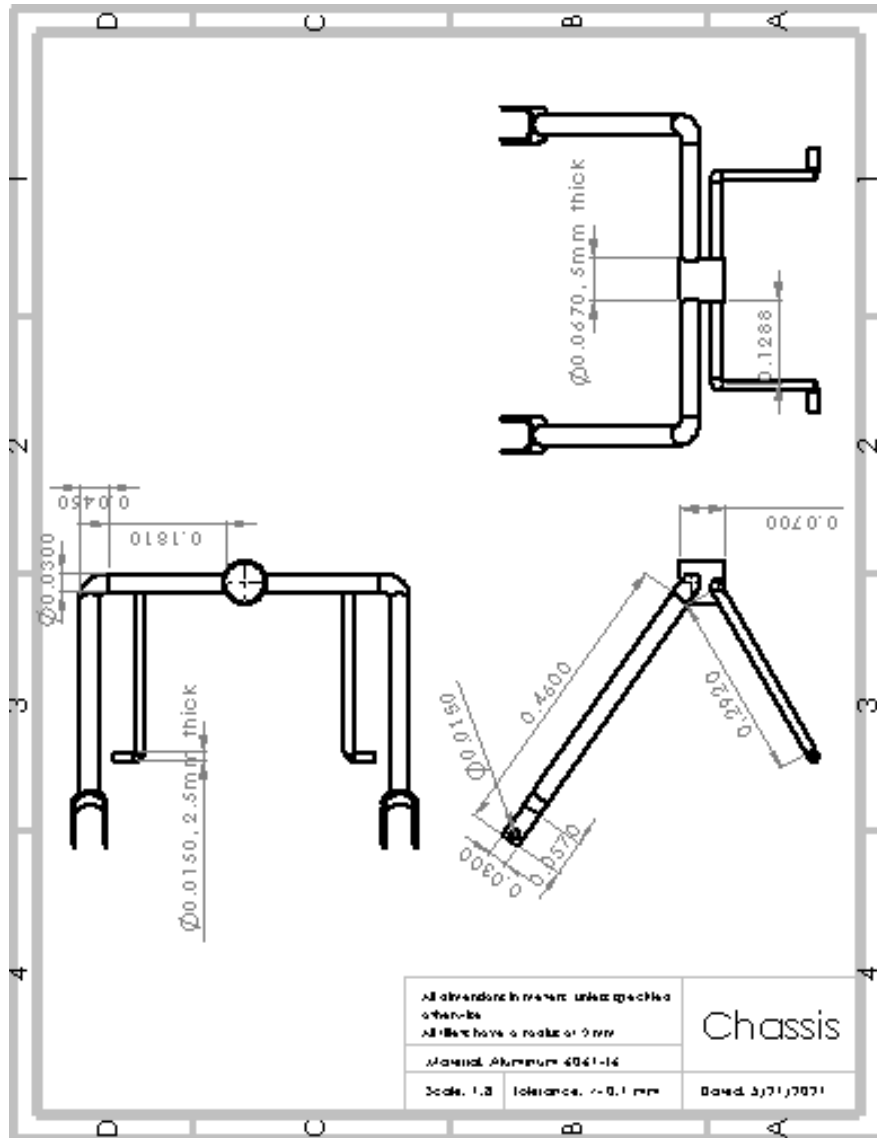Fig 46 below shows the drawing for chassis (including the stand).

Figure 46: Drawings of the Chassis

Steering

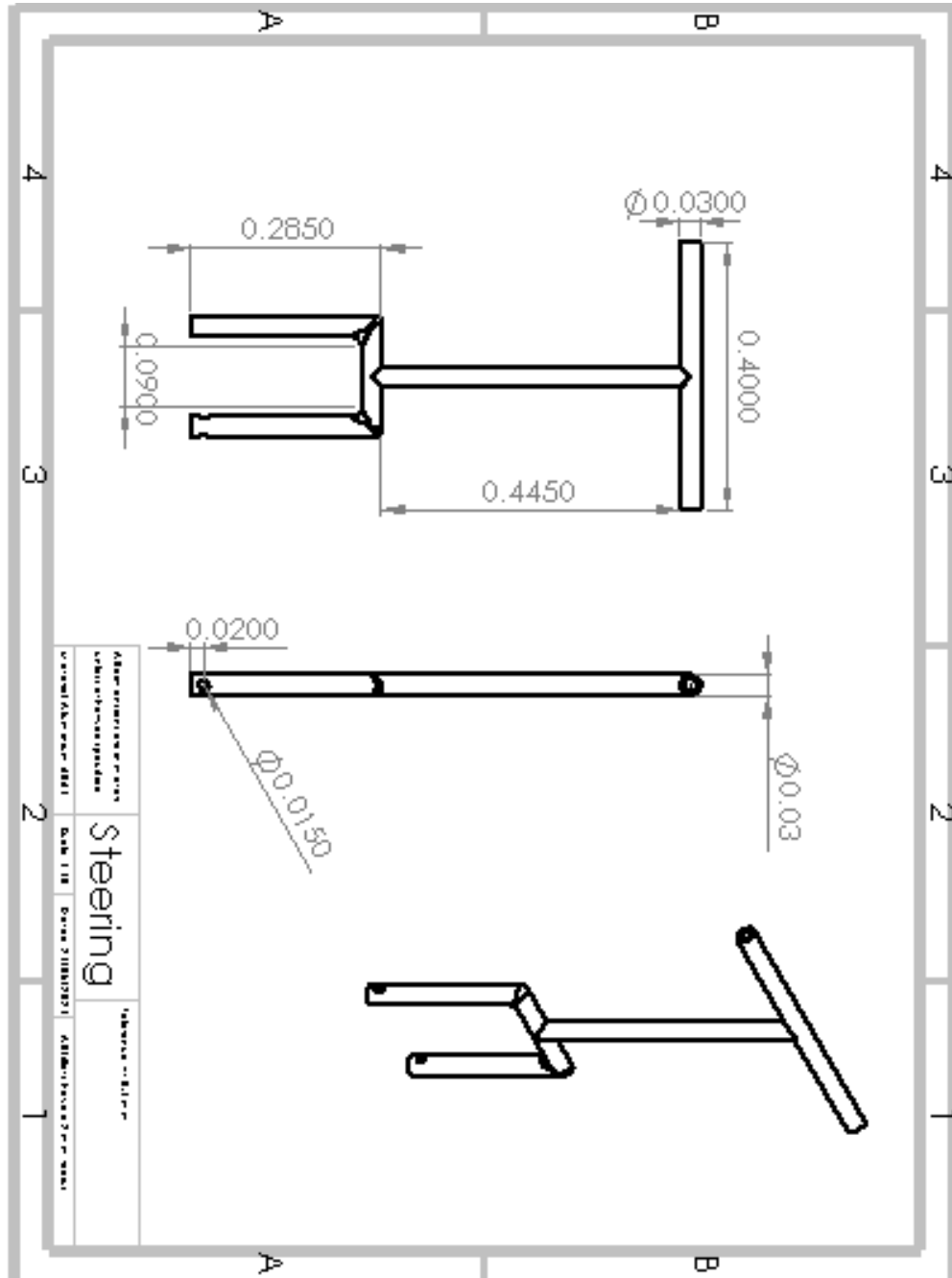Fig 47 below shows the drawing for the steering.

Figure 47: Drawings of the Steering

APPENDIX VI: DETAILED COST ANALYSIS

The manufacturing cost has been estimated using hourly rates for welders, sheet metal workers and lathe operators as shown in Table 23 below.

Table 23: Hourly Wage for the Manufacturing Labour

Worker	Payment (PKR Per Hour)	Time Required (Hours)	Total Payment (PKR)
Welder	200 [61]	2	400
Sheet Metal Worker	430 [62]	1	350
Lathe Operator	630 [63]	2	1300
Total			2090

The detailed cost analysis including various taxes (calculated using the calculator provided by FBR, Pakistan [64]) and shipping can be found in Table 24.

Table 24: Detailed Cost Analysis of the Product

Item	Aluminum	Hub Motor Tire with Disc Brakes	Bearing	Bolts, Nuts, Washers	Battery with Housing	Throttle	Manufacturing
-	Local	Imported	Local	Local	Imported	Local	-

HS Code	Cost (PKR)	Shipping	Custom Tax (%)	Sales Tax (%)	Income Tax (%)	Additional Sales	Total Tax (%)
-	400	0	0	0	0	0	0
8501.2	12920	836	0	17	11	2	32.4674
-	1895	0	0	0	0	0	0
-	300	0	0	0	0	0	0
8506.5	7448	532	3	17	11	2	36.441422
-	1785	0	0	0	0	0	0
-	2090	0	0	0	0	0	0

Cost After Tax (PKR)	Quantity	Total
400	5	2000
18222.21554	1	18222.21554
1895	1	1895
300	1	300
10888.02548	1	10888.02548
1785	1	1785
2090	-	2050
		~ 37180